Published in final edited form as:

Inorg Chem. 2023 December 18; 62(50): 20567–20581. doi:10.1021/acs.inorgchem.2c03931.

Sc-HOPO: A Potential Construct for Use in Radioscandium Based Radiopharmaceuticals

Michael D Phipps[1,2,3,4,a], **Shelbie Cingoranelli**[5,a], **N. V. S. Dinesh K. Bhupathiraju**[3], **Ali Younes**[2], **Minhua Cao**[2], **Vanessa A. Sanders**[4], **Michelle C. Neary**[2], **Matthew H. Daveny**[2], **Cathy S. Cutler**[4], **Gustavo E. Lopez**[1,3], **Shefali Saini**[5], **Candace C. Parker**[5], **Solana R. Fernandez**[5], **Jason S. Lewis**[6], **Suzanne E. Lapi**[5], **Lynn C. Francesconi**[1,2], **Melissa A. Deri**[1,3,*]

[1]Ph.D. Program in Chemistry, The Graduate Center of the City University of New York, New York, NY 10016

[2]Department of Chemistry, City University of New York Hunter College, 695 Park Avenue, New York, New York 10065

[3]Department of Chemistry, Lehman College of the City University of New York, Bronx, NY 10468

[4]Medical Isotope Research & Production Laboratory, Collider-Accelerator Division, Brookhaven National Laboratory, Upton, NY, 11973, USA

[5]Department of Radiology, University of Alabama at Birmingham, Birmingham, AL 35294

[6]Program in Molecular Pharmacology and Chemistry, Memorial Sloan Kettering Cancer Center, New York, NY 10065

Abstract

Three isotopes of scandium—^{43}Sc, ^{44}Sc, and ^{47}Sc—have attracted increasing attention as potential candidates for use in imaging and therapy, respectively, as well as for possible theranostic use as an elementally matched pair. Here, we present the octadentate chelator 3,4,3-(LI-1,2-HOPO) (or HOPO), an effective chelator for hard cations, as a potential ligand for use in radioscandium constructs with simple radiolabeling under mild conditions. HOPO forms a 1:1 Sc-HOPO complex that was fully characterized, both experimentally and theoretically. [^{47}Sc]Sc-HOPO has exhibited good stability in chemical and biological challenges over 7 d. In healthy mice, [^{43,47}Sc]Sc-HOPO clears the body rapidly with no signs of demetalation. HOPO is a strong candidate for use in radioscandium based radiopharmaceuticals.

Graphical Abstract

*Corresponding author: melissa.deri@lehman.cuny.edu.

[a] =Michael D Phipps and Shelbie Cingoranelli contributed equally to this work.

Supporting Information Available:

For further detail not shown in the body of this paper, please see the Supporting Information. There you will find experimental details for the synthesis of HOPO and additional characterization of the HOPO ligand and macroscopic Sc-HOPO. It also includes ^{44}Sc radiolabeling data, tabulated biodistribution data, and a GIF version of the dynamic PET image of [^{43}Sc]Sc-HOPO in healthy mice. This information is available free of charge at the website: https://pubs.acs.org/

Conflict of Interest statement

A patent on the bifunctional p-SCN-Bn-HOPO chelator has been filed with J.S.L., L.C.F, and M.A.D. as inventors.

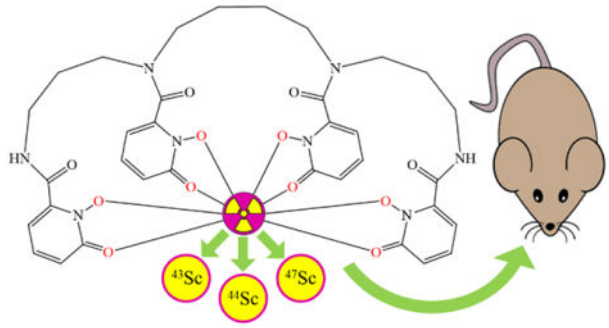

The 3,4,3-LI(1,2-HOPO) ligand can complex radioscandium for potential use in both diagnostic and therapeutic radiopharmaceuticals. The Sc-HOPO complex was evaluated both experimentally and computational to probe its structure and stability. Sc-HOPO demonstrates suitable stability over a range of chemical and biological conditions. We demonstrate radiolabeling under mild conditions with ^{43}Sc, ^{44}Sc, and ^{47}Sc. Radiolabeled [^{43}Sc]-HOPO and [^{47}Sc]-HOPO were evaluated *in vivo* for imaging and biodistribution and show rapid hepatobiliary excretion with no evidence of decomplexation.

Introduction

The strong appeal of personalized medicine has fueled expansion of the library of diagnostic and therapeutic agents that are tailored to optimize individual patient care. This goal has further driven research on the use of radiometals in medicine. Radiometals have a broad spectrum of both chemical and nuclear properties that provide many avenues for development of new radiopharmaceuticals with different clinical utilities. To date, research into radiometal based radiopharmaceuticals has yielded FDA approved agents for both imaging and therapy with several radiometals, including ^{99m}Tc, ^{68}Ga, ^{111}In, ^{177}Lu, ^{90}Y, and more.[1] There are numerous other agents incorporating radiometals either in clinical trials or under investigation.

The chemical and nuclear properties of a specific radiometal determine its suitability for incorporation into a radiopharmaceutical agent. For example, the type of radioactive decay the radiometal undergoes and its half-life determine its potential medical application. The chemistry of the radiometal governs its stable inclusion in a chelator in the drug and the biological effects should it be released from the chelator. One radiometal recently attracting attention is scandium because it has several accessible isotopes with medical utility, including ^{43}Sc, ^{44}Sc, and ^{47}Sc. ^{43}Sc ($t_{1/2}$ = 3.89 h, β^+_{max} = 1.20 MeV, $BR_{\beta+}$ = 70.9%) and ^{44}Sc ($t_{1/2}$ = 3.97 h, β^+_{max} = 1.47 MeV, $BR_{\beta+}$ = 94.3%) have emission properties that make them a suitable for use in positron emission tomography (PET) imaging.[2] ^{47}Sc ($t_{1/2}$ = 3.35 d, β^-_{max} = 0.6 MeV, $BR_{\beta-}$ = 100%) has emission properties suitable for targeted radiotherapy and radioimmunotherapy (RIT) and also possesses a single gamma emission (159 keV, BR_γ = 68%) that is similar to ^{99m}Tc (140 keV, BR_γ = 89%) and has the potential for application in single photon emission computed tomography (SPECT) imaging. In combination, these different radioisotopes of scandium can be used to create chemically identical radiopharmaceuticals that can be used for both therapeutic

and diagnostic applications, i.e., theranostic agents. Additionally, since ^{47}Sc alone has both therapeutic β^- and imageable γ emissions, it can be used toward the development of a single true theranostic agent.[2]

The half-lives of ^{43}Sc and ^{44}Sc render them appropriate for use with small molecules and peptides, whose *in vivo* kinetics are faster than monoclonal antibodies (mAbs), or with pretargeted strategies using mAbs. The longer half-life of ^{47}Sc is appropriate for use with mAbs in radioimmunotherapy (RIT), as radioimmunoconjugates may need to circulate for a few days before accumulating at their target. The longer half-life does not preclude it from use in pretargeting, and so $^{43/47}$Sc or $^{44/47}$Sc could both be used in a pretargeted theranostic system with the nuclides being exchanged in either diagnostic or therapeutic context, respectively.

Radiometals require a chelator for stabilization and incorporation into a pharmacophore. The role of the chelator is to bind the radiometal and ensure a stable complex, at least until the biological target is reached. The 1,4,7,10-Tetraazacyclododecane-1,4,7,10-tetraacetic acid (DOTA) ligand is considered a relatively universal chelator and has been used for a variety of radiometals, including ^{177}Lu, ^{68}Ga, and ^{90}Y clinically. DOTA has been used to create and evaluate radioscandium based constructs in both preclinical work and early clinical work.[3–11] Recently, the production and accessibility of a wider library of radiometals prompted demand for new chelators designed with their particular chemistry in mind.[12, 13]

In some cases, the conditions needed for the chemical synthesis of radiometal complexes is incompatible with the conjugated targeting molecule. For example, syntheses with DOTA conjugates generally employ reaction temperatures of 60–95 °C that are incompatible with mAbs.[7, 8, 14, 15] Overcoming this obstacle involves drawbacks such as longer synthesis time that is detrimental to nuclides with short half-lives, prolonged exposure to workers, and potential degradation of the functional group that conjugates to the protein.

Sc is the first transition metal and is a part of the rare earth elements (REEs). It forms a trivalent ion with coordination chemistry similar to other REE ions such as Y^{3+}, with a preference for octadentate coordination complexes. Sc^{3+} is a small, hard ion with a preference for hard donor groups such as O or N. So far, radioscandium complexes have been reported with both cyclic and acyclic polyamino-polycarboxylate chelators.[4, 16–21] A significant portion of radioscandium *in vivo* work has been performed with small molecule conjugates using DOTA as the chelator.[8, 15] These studies have used small molecules as targeting vectors, including DOTA-octreotate (DOTATATE), prostate specific membrane antigen (PSMA), and folate, that can be labeled at high temperatures. At lower labeling temperatures, there is the risk for the formation of “out-of-cage” complexes where a metal cation is bound by the oxygens on the pendant arms, but not within the N_4 ring of the ligand, thus compromising the stability of the construct and increasing the likelihood of the metal being released.[4] Other chelators such as CHX-A″-DTPA, AAZTA, and H_3mpatcn have been used for *in vivo* studies as well.[19–21] Both CHX-A″-DTPA and H_3mpatcn have exhibited radiolabeling at room temperature. Investigation of a variety of “old” and “new” ligands will allow development of a better optimized chelate system for efficient labeling under mild conditions and for increased complex stability.

3,4,3-(LI-1,2-HOPO) (or HOPO, Figure 1) is an acyclic chelator that has demonstrated a strong affinity for hard metal +3 and +4 ions.[22–26] It has been previously demonstrated as a superior chelator for ^{89}Zr with less *in vivo* demetalation than ^{89}Zr-DFO, the clinically used chelator. HOPO is an 8-coordinate ligand with hard oxygen donating groups which are suitable for Sc^{3+} ion which typically produces 8-coordinate complexes, with 7 and 6 coordinate species also known.[27–29] HOPO has also been demonstrated to form complexes with metals at a lower pH than DOTA, and the acyclic arrangement should result faster binding kinetics compared to a macrocycle. A bifunctional *p*-SCN-Bn-HOPO that can be conjugated to biomolecules has previously been developed, evaluated, and synthetically optimized.[23, 30]

In this study, we investigate the radiolabeling, characterization, stability, and *in vivo* behavior of [$^{43/44/47}$Sc]Sc-HOPO as well as the synthesis and characterization of the macroscopic Sc-HOPO complex. These experiments demonstrate the potential for HOPO as a chelator for the development of radioscandium based agents.

Results and Discussion

The design and selection of chelators for radioscandium should focus on best meeting the specific chemical properties of the Sc^{3+} ion. Our criteria for an ideal chelator for scandium are as follows. An octadentate ligand offers the potential to fully saturate the coordination sphere of Sc^{3+}. Hard oxygen donor groups are desirable to complement the hard Sc^{3+} cation. The chelator must also have a properly sized cavity for the 1.01 Å effective ionic radius for 8-coordinate Sc(III).[31] Acyclic chelators are preferred because their flexibility should facilitate faster kinetics for more efficient radiolabeling conditions. By combining these properties within one molecule, the HOPO ligand is a strong candidate as a potential chelator for Sc^{3+}. Herein, we've paired our macroscopic characterization, radiochemistry, and stability studies with DFT studies to confirm the performance and stability of the Sc-HOPO complex.

Synthesis

The HOPO ligand was synthesized as previously reported with minor augmentations.[24, 32, 33] The final product was reverse-phase HPLC purified to remove trace impurities that could potentially interfere with radiolabeling. The synthesis is given in the Supporting Information, Scheme S1 and Figure S1.

The symmetry and flexibility of HOPO result in an ^{1}H NMR spectrum with many overlapping multiplets and broad peaks due to coexisting conformers in solution. Mass spectrometry and HPLC analysis, Figures S2A and S3A, respectively, corroborate HOPO as a single compound. HOPO picks up Fe(III) very easily and therefore it is common to observe Fe-HOPO in the LCMS.[34]

Non-radioactive, macroscopic Sc-HOPO was synthesized and characterized for comparison with the tracer Sc-HOPO. $ScCl_3$ was added to an aqueous solution of HOPO in a 1:1.1 ratio of HOPO to Sc in water at room temperature. Upon the addition of $ScCl_3$ to the solution of HOPO, a white precipitate formed almost immediately, and the solution became milky.

The Sc-HOPO complex has relatively low solubility, especially under acidic conditions. The precipitate redissolved as the pH was raised by the addition of K_2CO_3. If the pH rises above 7 and becomes basic, a new precipitate will form. This is unreacted Sc precipitating as $Sc(OH)_3$, which is insoluble under mildly basic conditions. The reaction mixture was filtered through a 0.2 μm syringe filter to remove the $Sc(OH)_3$. The resulting complex of Sc-HOPO carries a charge of −1, and so K_2CO_3 was also used to provide a K^+ counter-ion to the complex. The filtered solution was then lyophilized to dryness. K[Sc(HOPO)] was purified by reverse-phase HPLC, and lyophilized to a powder.

Characterization:

High resolution mass spectrometry (HRMS) of the product dissolved in water identifies the Sc-HOPO complex with the expected mass signals (793.2008 Da for $[M+2H]^+$ and 815.1821 Da for $[M+H+Na]^+$) (Figure S2B). Analytical HPLC of the product dissolved in water shows a peak at retention time 5.35 minutes that tails slightly with another small peak at 6.29 minutes (Figure S3B). The HPLC and LC-MS chromatograms both exhibited a long tail following the primary peak. Mass analysis of the primary peak and tail region indicates that only the mass of Sc-HOPO is present in all regions of the tail and primary peak. This indicates the presence of alternative species of the Sc-HOPO that interacts slightly differently with the column. An alternative Sc-HOPO species was indicated in ^{1}H NMR studies as a function of pH and the formulation of the potential species was examined by DFT calculations, *vide infra*.

Figure 2 shows the ^{1}H NMR of Sc-HOPO and the HOPO ligand in D_2O at pH 7. The ^{1}H NMR of the Sc-HOPO complex showed overlapping multiplets in the aliphatic region similar to the ^{1}H NMR of HOPO, however with less broadness. The peaks in the aromatic region, most associated with the binding of the hydroxypyridinonates to Sc^{3+}, experienced the most significant change, with clean, discrete peaks indicative of binding to the metal center, locking the electronic environments of those protons. This is in contrast to the ^{1}H NMR spectra of Zr-HOPO described by Deri et al, where the aromatic region showed a complex set of overlapping multiplets.[24]

^{45}Sc is a quadrupolar nucleus that is easily probed even at low concentrations by ^{45}Sc NMR due to its sensitivity. Additionally, it is monoisotopic, so there are no other isotopes of Sc macroscopically to dilute an NMR signal. ^{45}Sc NMR (Figure 3) shows a single broad peak at δ 62.38 ppm with a large FWHM of 12414 Hz that is consistent with other Sc chelate compounds, such as Sc-DOTA, Sc-DTPA, Sc-EDTA, Sc-AAZTA, and Sc-mpatcn.[18, 20, 35, 36] The analysis of liquid samples of Sc chelates by ^{45}Sc NMR tends to give broad peaks that are shifted down range (> 50 ppm) from the reference. The broadness may result from the asymmetry of the ligand field in Sc-HOPO compared to the highly symmetric $Sc(H_2O)_6^{3+}$ ion in the reference standard. As ^{45}Sc is a quadrupolar nucleus, peak broadening is expected in the case of asymmetric ligand fields. An asymmetric ligand can arise from a non-fluxional environment of the chelate, which is expected from the 8-coordinate structure provided by the chelation of Sc(III) by HOPO.[18, 37, 38] This has been observed in the comparison of Sc-DTPA and Sc-DOTA systems.[18, 35, 37, 38] The chemical shift is consistent with full encapsulation of the Sc^{3+} nucleus by the hydroxypyridinonate groups, resulting in the Sc^{3+}

nucleus being highly shielded. The formation of “out-of-cage” complexes tends to give shifts in a lower range of 20–30 ppm.[4, 18, 39] A lower chemical shift in this range is due in part to the poor shielding of the Sc^{3+} nucleus from solvent molecules in comparison to a fully chelated metal center without coordinating solvent molecules.[4, 20] Additionally, it is expected to see more narrow peak width in the case of out-of-cage complexes that see a more fluxional environment.[18, 35] This downfield broad peak observed for the Sc-HOPO sample supports the identification as an in-cage, asymmetric single structure. Hence, the ^{45}Sc NMR evidence indicates the complete chelation of the Sc^{3+} nucleus by the HOPO chelator.

A K[Sc(HOPO)] crystal structure was obtained previously by Carter et al which contained DMF in the lattice.[40] In this work, crystals of K[Sc(HOPO)] in the form of $\{K(OH_2)_2[Sc(HOPO)]\}_2$ were obtained by slow evaporation of a solution of K[Sc(HOPO)] with K_2CO_3 and KCl in water over 8 weeks without any DMF present. A single crystal from this sample was taken and analyzed by X-ray crystallography. The details of the crystal, intensity collection and refinement data are shown in Table S1. Relevant bond lengths and angles are shown in Table S2. The crystal structure is shown in Figure 4. The resulting structure is a racemic pair of enantiomers in a Monoclinic space group (*$P2_1/c$*) with only H_2O in the lattice, in contrast to the Carter et al. structure which contained a racemic pair of Sc-HOPO units in a Triclinic space group (*P-1*) with both H_2O and DMF. There are, however, some similarities in the complexes themselves. Both structures display a racemic pair of an 8-coordinate Sc-HOPO complex with a distorted square antiprismatic geometry around the metal center. In this structure, two enantiomeric Sc-HOPO units are bridged by two K^+ units. The complexes exhibit Δ(δ) and Λ(λ) handedness according to the orientation of the butylene diamine portion of the ligand backbone relative to the metal center. Such isomerism has been observed in other metal complexes with HOPO, such as in Zr-HOPO.[23] As noted by Carter et al, it has yet to be determined if the enantiomers of Sc-HOPO are separable.[40] There is a small amount of disorder in the flexible alkyl backbone of the ligand, as well as disorder from the solvent and K-bridges. The average Sc-O bond length was 2.221 Å, which is slightly longer than the 2.213 Å average bond length reported by Carter et al.[40] The small difference in reported average bond length may be related to the different packing conditions of the crystals. There was no clear pattern regarding the differences in individual Sc-O bond lengths, which ranged from 2.1790(17) to 2.2658(17) Å. The inner and outer hydroxypyridinonate groups on either side of the metal center each bind to Sc opposite from its corresponding hydroxypyridinonate group on the other half of the ligand; the inner hydroxypyridinonate groups are opposite one another, and the outer hydroxypyridinonate groups are opposite one another. An isomer where an inner and outer hydroxypyridinonate group are opposite one another around the Sc center has not been observed. This product may not form due to steric hinderance from the bending of the backbone that would occur in that case. Corroborating the overall connectivity and structural features of the Sc-HOPO anion, this structure was the basis for successful DFT calculations, *vide infra*.

FT-IR and UV-vis spectra of HOPO and Sc-HOPO were measured and compared. These can be found in Figure S5 and Figure S6 respectively. FT-IR samples were solid powders pressed under a mechanical arm for attenuated total reflectance (ATR). In the FT-IR spectra, peak changes from HOPO to Sc-HOPO (1633 cm^{-1} to 1610 cm^{-1}, 1529 cm^{-1}

to 1515 cm^{-1}) are characteristic of redshifting in carbon-oxygen vibrations that occur when hydroxypyridinonate binds a metal.[24] The UV-vis experiments were done on liquid samples at pH 7. This also shows redshifting in the absorbance maxima between HOPO and Sc-HOPO. HOPO has maxima at 222 nm and 308 nm, while Sc-HOPO has maxima at 226 nm and 315 nm.

Proton NMR as a function of pH suggests minor species at low pH

As the pH is decreased from 8 to 2, broad and poorly defined peaks grow in the ^{1}H NMR (Figure 5), indicating a minor species growing in as the acid content increases. This minor species exists in equilibrium with the dominant Sc-HOPO species under acidic conditions and thus could not be isolated and analyzed separately. The low solubility of Sc-HOPO under acidic conditions also contributed to the poor resolution of the peaks in the minor species. Stability constant measurements and the speciation diagram reported by Carter, et. al. suggest that this minor species is very likely Sc-HOPO with the addition of a proton. In that study, the protonated Sc-HOPOH species forms in the pH region of −2 to 4.[40] Our NMR data is consistent with Sc-HOPOH existing as a minor species at pH 2. Below pH 2, we encountered solubility issues in our sample that made us unable to collect suitable ^{1}H NMR spectra at lower pH's because there would be too little sample in solution.It is important to note that this process is reversible: increasing the pH to neutrality, returns the ^{1}H NMR spectrum to the original spectrum at pH 8. This reversible speciation change, as a function of pH, underlies the stability of the Sc-HOPO species. The use of DCl and K_2CO_3 to adjust the pH of the ^{1}H NMR samples resulted in the presence of KCl in solution. This varying concentration of KCl in the samples resulted in minor chemical shift changes of the peaks; the other features of the peaks remained the same. The effects of salt concentration on the chemical shift of the signals were verified by ^{1}H NMR following the addition of KCl to Sc-HOPO samples without altering the pH. This speciation is also reflected in the HPLC data where an acidic mobile phase is employed (0.1% TFA). In the HPLC data, *vide supra*, the major peak tails into a second minor Sc-HOPO species.

Proposed structures for the conformations of this protonated species are shown in Figure 6. In one case the hydroxyl group on an "outer" hydroxypyridinonate group is protonated and released from the Sc center to form a 7-coordinate complex (Figure 6B). In the second case, the hydroxyl group on an "inner" hydroxypyridinonate group is protonated and released from the Sc ion (Figure 6C). Both scenarios would result in flexible constructs that would manifest as broad peaks in the NMR spectrum. DFT calculations were employed to interrogate these species further.

DFT Calculations

Figure 7 shows the lowest energy equilibrium structures of the 8- and 7-coordinate complexes. For these calculations, only one isomer from the racemic mixture was considered for the optimized structures and reaction energetics. This was chosen in part for simplicity because the isomers should be nearly identical regarding their bond distances and energetics within a protonation reaction. Like the crystal structure, the optimized 8-coordinate complex (Figure 7A) has a distorted square antiprismatic structure around the Sc center; the Sc is coordinated to the eight oxygens from the four hydroxypyridinonate

units of the HOPO. Table 1 shows that the average Sc-O bond for the 8-coordinate complex (A) is 2.25 Å, which is similar to the value obtained for the crystal structure (2.21 Å). Figure 7B and 7C show the optimized structures for the 7-coordinate B and C complexes, where a proton is located on the outer and inner hydroxypyridinonate moiety, respectively. From Table 1, we notice that in the 7-coordinate complex C, the distance between the H in the protonated hydroxypyridinonate and the O in the adjacent hydroxypyridinonate is 1.98 Å, and the angle between the OH in the protonated hydroxypyridinonate and the O in the adjacent unprotonated hydroxypyridinonate is 15° – signaling the formation of a hydrogen bond. In the case of 7-coordinate B complex, the formation of a hydrogen bond is not observed.

Table 2 shows the changes in electronic energy and thermodynamic properties for the formation of the complexes (reactions 1 and 2, see Materials and Methods). For the 8-coordinate complex (A) it can be observed that ΔE_e and ΔG_s in solution are < 0, suggesting that this complex is stable electronically and thermodynamically. Moreover, $\Delta H_s < 0$ and $\Delta S_s > 0$, indicating that the 8-coordinate complex is stabilized by both energetic and entropic contributions. Although smaller in magnitude, the same electronic and thermodynamic stabilization is observed for the 7-coordinate complexes. In this case, the 7-coordinate complexes are thermodynamically stabilized by only the enthalpic contribution. The 7-coordinate C complex is 5.5 kcal/mol more stable than the 7-coordinate B complex. This suggests that the minor species observed in the NMR, HPLC, and from stability constant measurements is the 7-coordinate protonated species C. The enhanced stability of complex C over B can be attributed to the formation of a H bond between the protonated N on the hydroxypyridinonate and the O on the adjacent inner hydroxypyridinonate.

For the 7-coordinate Sc complexes, additional calculations were performed with an additional H_2O or OH placed in the proximity of the Sc as to allow for the formation of an 8-coordinate complex. In all cases, the H_2O or OH did not coordinate to the Sc, but rather remained unbound to the complex.

The last column in Table 2 shows the HOMO-LUMO energy gap (energy difference between the LUMO and the HOMO) and Figure 8 show the orbital energy level diagram for each complex. As expected for molecules with highly delocalized π orbitals, the energy gap is relatively large.[41] However, the energy gap of the 7-coordinate C complex is approximately 0.5 eV larger than the 7-coordinate B complex. As previously discussed elsewhere[41, 42], a larger energy gap implies a more stable system. Hence, the 7-coordinate C complex is more stable than the 7-coordinate B complex in terms of the energy gap – in agreement with our electronic structure energy differences and thermodynamic results.

When the frontier orbitals for the complexes are examined, several interesting features can be observed. For the HOMO, i) the 8-coordinate complex has the electronic cloud equally distributed between the four hydroxypyridinonate moieties, with only an 18 % contribution of the Sc, ii) the 7-coordinate complexes have the electron cloud distributed between three hydroxypyridinonate groups, with the one not having electron density being the protonated hydroxypyridinonate. It can be noticed that the contribution of the metallic orbitals is less in 7-coordinated complex C than the other two complexes. In the case of the LUMO all

complexes show the same electronic distribution, located in one of the hydroxypyridinonate groups and only a 10 % contribution of the p-orbital of the Sc.

Radiolabeling

^{44}Sc was obtained in 2 M HCl from a ^{44}Ti/^{44}Sc generator system, evaporated to dryness, and reconstituted in 100 mM ammonium acetate solution at pH 5. Radiolabeling was performed in pH 5 ammonium acetate buffer with 250 μM ligand, either DOTA or HOPO. The reactions were shaken for 30 min with DOTA heated at 95 °C, and HOPO heated at 37 °C. The TLC results from the radiolabeling can be found in Figure S8. The plastic backed silica gel TLC were developed using 50 mM EDTA at pH 5. Under these conditions, “free” ^{44}Sc should be captured by EDTA and move with the solvent front. The radio-TLC of free ^{44}Sc shows a portion of the activity bound to the origin. This is the result of the formation of oxides or hydroxides of Sc precipitating out of the solution as insoluble particles that stick to the origin on the TLC plate. These particles form under elevated pH conditions and can be difficult to avoid when adding radioscandium from the acidic solution collected from radionuclidic purification to the buffer solution used in radiolabeling. These particles may sometimes be recovered by dissolution in concentrated HCl. However, activity loss from oxide formation may be irreversible. Both cases have been observed when radiolabeling with radioscandium. Harshly raising the pH of the solution containing radioscandium causes more particle formation. Particle formation also appears to worsen with the age of the radioscandium solution. The use of a minicentrifuge, 0.2 μm syringe filter, nor C18 sep-pak were effective to remove particles. We consider that the size of the particles at the tracer level made these methods ineffective. The [^{44}Sc]Sc-DOTA and [^{44}Sc]Sc-HOPO complexes migrate with an R_f of 0.2 that is separated from the ^{44}Sc oxides. [^{44}Sc]Sc-DOTA and [^{44}Sc]Sc-HOPO both labeled with >95% radiolabeling yield.

^{43}Sc and ^{47}Sc were collected in 0.1 M HCl, evaporated to dryness and reconstituted in 0.25 M ammonium acetate solution pH 4. HOPO and DOTA were labeled with radioscandium in 0.25 M ammonium acetate buffer at pH 4 at 37 °C and pH 4 at 95 °C respectively. Yields were > 95% as determined by ITLC-SG strips in 50 mM EDTA. The free radioscandium moved completely with the solvent front while labeled constructs moved with an R_f value of 0.65. Reactions at more acidic pH’s as well as at RT were tried to determine the boundaries of viable radiolabeling conditions. Labelling of HOPO was achieved at RT and pH 7 (>95%) while DOTA did not show any radiolabeling. Up to 80% RCY were obtained with HOPO at pH 1 and 37°C while DOTA did not label at all.

A coelution of [^{47}Sc]Sc-HOPO with characterized macroscopic Sc-HOPO was performed (Figure 9). An aliquot (~1 uCi) of radiolabeled [^{47}Sc]Sc-HOPO was added to a solution containing 10 mM Sc-HOPO. The elution profiles match well. There is a slight lag time between the profiles from each detector due to the distance between the UV and radiation detectors. This coelution demonstrates that the [^{47}Sc]Sc-HOPO possesses the same structure and chemistry, including the minor protonated species, that was found for the macroscopic Sc-HOPO, thus validating the synthesis of the desired [^{47}Sc]Sc-HOPO in the radiolabeling reaction.

Stability Studies

To assess stability of radioscandium complexes over time, [^{47}Sc]Sc-DOTA and [^{47}Sc]Sc-HOPO were subjected to studies where the complexes were “challenged” with EDTA, pH, and other metal ions.

The [^{47}Sc]Sc-DOTA and [^{47}Sc]Sc-HOPO stability challenges with EDTA both showed high stability, >93% for [^{47}Sc]Sc-HOPO for all constructs and 100% for all [^{47}Sc]Sc-DOTA constructs as shown in Figure 10 attesting to the high stability of the ^{47}Sc constructs.

The [^{47}Sc]Sc-DOTA complex remained 100% intact at pH: 5, 6, 7, 8. The [^{47}Sc]Sc-HOPO shows similar robustness as most complexes remain 100% complex over the course of the 7 days with a slight decrease at pH 6 (93%). These results show that HOPO is a comparable chelator to DOTA in the presence of EDTA.

Additional studies examined the influence of other metal ions to the chelators. Figure 11 below represents the results of the metal challenge for DOTA and HOPO complexes.

[^{47}Sc]Sc-DOTA is stable in the presence of iron, copper and magnesium out to 7 days. In the [^{47}Sc]Sc-HOPO metal challenge, HOPO is shown to de-complex in the presence of iron and copper within the first day. Both complexes are shown to be unstable in the presence of zinc, with HOPO de-complexing within the first hour and DOTA beginning to de-complex within the first day. Although DOTA outperformed HOPO in this study, this study employed relatively extreme chemical environments that are not representative of biological conditions or the concentrations of competing metal ions that would be found there. Therefore, it is not predictive of the behavior of [^{47}Sc]Sc-HOPO *in vivo*. To better probe *in vivo* behavior, biodistribution studies were conducted.

Biodistribution

Four groups (n=4) of mice were injected with 10 μCi of [^{47}Sc]Sc-HOPO and biodistributions were performed at various time points. Figure 12 below represents the average biodistribution of four mice at 10 minutes, 1 hour, 4 hours, and 24 hours after injections.

The results, shown in Figure 12 and Table S3, demonstrate that [^{47}Sc]Sc-HOPO is excreted via the hepatobiliary pathway. Within the first 10 minutes, the complex is shown to have significant uptake in the small intestines. The 1- and 4-hour biodistribution shown the complex moving into large intestines. The %ID/g from 1-hour to 4-hour mark also decreases, indicating that the complex is being excreted from the mouse as the other organs do not show significant uptake at both time points. Furthermore, the 24-hour time point has a lower %ID/g (20% at 4-hours to 2% at 24-hours), indicating that the majority of the complex is largely excreted.

Another biodistribution was performed on mice injected with [^{43}Sc]Sc-HOPO to further validate the biodistribution pattern and determine suitability for PET imaging. The [^{43}Sc]Sc-HOPO biodistribution data, shown in Table S4, exhibits the same trend with the complex moving from the small intestines into the large intestines. From both biodistributions, the

[^{43,47}Sc]Sc-HOPO complexes show uptake and excretion through the gastrointestinal tract. Another animal study was performed with free ^{47}Sc to compare to the biodistribution of [^{43,47}Sc]Sc-HOPO. Free ^{47}Sc in saline was injected into a set of mice (n=4) and biodistribution was performed at 1 hour for direct comparison to the 1 hour biodistribution timepoint of [^{47}Sc]Sc-HOPO. These data are shown in **Table S6**. The free ^{47}Sc has a more widespread uptake within heart, lungs, spleen, kidney, and femur. The [^{43,47}Sc]Sc-HOPO complex does not follow the same distribution path as free ^{47}Sc and shows uptake and excretion almost exclusively via the gastrointestinal path. This further validates the chemical inertness of the [^{43,47}Sc]Sc-HOPO *in vivo*.

PET Imaging

Additional evaluation of the *in vivo* stability for the [^{43}Sc]Sc-HOPO complex was determined by PET imaging in normal mice. Standard uptake value (SUV) data show a low time activity curve for brain, lung, kidney, heart, and liver (Figure 13). The liver and kidney SUV decrease throughout the study in support of the previous data showing the complex moving through the gastrointestinal tract. The SUV data mirror the biodistribution data as the uptake for each organ was significantly lower than the intestines. Furthermore, the Maximum Intensity Projection (MIP) image of the Balb/c mice (Figure 14) clearly shows excretion through the hepatobiliary tract and no uptake in the blood, lung, heart, kidneys, or femur that was observed in the biodistribution of free ^{47}Sc, complimenting the biodistribution data of [^{47}Sc]Sc-HOPO discussed above. Both *in vivo* experiments show the chemical robustness of the [^{43,47}Sc]Sc-HOPO.

The data does not indicate decomplexation due to the absence of high uptake in blood, lung, heart and kidneys shown in both biodistribution and dynamic image. Comparison with free ^{47}Sc *in vivo* was used to verify the inertness of the complex. Free ^{47}Sc in saline was injected into a set of mice (n=4) and biodistribution was performed at 1 hour for direct comparison to the 1 hour biodistribution of [^{47}Sc]Sc-HOPO. The complexes have excretion through the hepatic tract (liver, small and large intestines) while free [^{47}Sc]$ScCl_3$ has a widespread biodistribution with uptake seen in heart, spleen and kidneys along with the liver, and intestines as seen in Table S5.

Conclusions

The 3,4,3-(LI-1,2-HOPO) ligand has been shown to be a suitable chelator for Sc^{3+}, and evidence presented here indicates that it is a comparable chelator to DOTA for Sc^{3+}. We synthesized and characterized the macroscopic Sc-HOPO complex. The Sc-HOPO complex exhibits an expected octadentate structure with a pair of enantiomers. The Sc^{3+} center is bound to all 8 of the coordinating oxygens from the 4 hydroxypyridinonate groups on the ligand. Additionally, the complex experiences a reversible protonation beginning below pH 4 as shown through pH dependent NMR studies, observed in the HPLC and LC-MS profiles, and corroborated by DFT studies. This is consistent with stability constant data reported by Carter, et. al.[40] The reversible nature of this protonation without any disruption to the complexation of Sc attests to the stability of the Sc-HOPO complex.

Radiolabeling experiments were carried out to synthesize the [^{43,44,47}Sc]Sc-HOPO complexes. The low pK_a's for HOPO enable it to be radiolabeled at lower pH compared to DOTA which are more compatible with biological targeting vectors. The stability of the [^{43,47}Sc]Sc-HOPO complexes was demonstrated by *in vitro* studies and *in vivo* biodistribution and imaging studies. The *in vitro* experiments demonstrate that HOPO possesses comparable stability to DOTA. The fast kinetics of labeling the HOPO ligand with radioscandium at mild temperatures may offer an advantage over DOTA and other macrocycles. Although acyclic chelators tend to have lower thermodynamic stability than their macrocyclic chelators, HOPO demonstrated stability that matches DOTA under the various conditions of the experiments conducted here. Furthermore, *in vivo* application of [^{43,47}Sc]Sc-HOPO indicates the complex is excreted through the intestinal tract and in contrast to the biodistribution of free ^{47}Sc, where there is significant uptake in the heart, lungs, spleen, kidney, and femur. Accordingly, there is no indication of decomplexation of the [^{43,47}Sc]Sc-HOPO. Overall, this study demonstrates the viability of the Sc-HOPO complex as a potential construct for radioscandium-based agents and paves the way for future work with bifunctional HOPO variants for targeted imaging and therapy.

Experimental

Materials and Methods

All radioactive work was done in approved laboratories to handle low levels of radioactivity for gamma and beta emitters with appropriate safety training and radiation monitoring. All chemicals were purchased from Fisher or Sigma-Aldrich and used without purification. All water was ultrapure (> 18.2 MΩ). Instruments were calibrated and maintained according to standard quality control procedures. Compounds were analyzed by liquid chromatography high-resolution mass spectrometry (LC-HRMS). LC-HRMS was performed on an Agilent 6550 iFunnel Q-TOF mass spectrometer coupled to an Agilent 1290 Infinity LC system (binary pump, diode array detector, and autosampler). Chromatography was performed using an Agilent SB-C8 column (2.1 × 50 mm) at 45°C and a gradient of solvents A (water, 0.1% formic acid) and B (acetonitrile, 0.1% formic acid) from 2 to 98% solvent B in 10 min at a flow rate of 0.2 mL/min. The following settings were applied to the ESI source: gas temperature, 250°C; nebulizer, 30 psig; sheath gas temperature, 250°C; Vcap, 3500 V; and nozzle voltage, 2000 V. For MS analysis, full scan mass spectra (m/z = 100–3000) were acquired in positive-ion mode. Data were acquired and analyzed using Agilent's MassHunter Software suite (Data Acquisition B.09.00, Qualitative Analysis B.07.00). ^{1}H NMR experiments were performed on a Bruker Avance III 600 MHz NMR Spectrometer with data processed by Topspin 4.1.4 software. ^{45}Sc NMR experiments were performed on a Bruker Avance III 400 MHz NMR Spectrometer. NMR spectra are expressed on the δ scale. NMR spectra were referenced to solvent peaks or 3-(trimethylsilyl)-1-propanesulfonic acid, sodium salt (DSS). Measurement of pH was performed on a Fisherbrand Accument™ AE150 pH meter with a Fisherbrand™ accumet™ Micro Glass Mercury-Free Combination Electrode. The HPLC system used for analysis and purification of macroscopic material was a Shimadzu Prominence system equipped with a diode array and an automatic fraction collector. HPLC purification was performed with a Shimadzu GIST Shim Packed C18 Semi-preparative 10 × 250 mm column, and analysis was performed on a Kromasil

Universal C18 4.6 × 250 mm column. UV-vis spectroscopy was performed on a Thermo Evolution 220 UV-Visible Spectrophotometer. Infrared attenuated total reflectance (IR-ATR) spectroscopy was performed on a PerkinElmer Spectrum 2 FT-IR spectrometer with a Universal ATR Sampling Accessory. X-ray diffraction data were collected on a Bruker X8 Kappa Apex II diffractometer using Mo Kα radiation. ^{44}Sc was obtained at Brookhaven National Laboratory (BNL) from a ^{44}Ti/^{44}Sc generator. Enriched [^{46,50}Ti]TiO_2 was obtained from the Department of Energy. Proton irradiations were performed on TR-24 cyclotron (Advanced Cyclotron Systems (ACSI, INC)). Activity measurements were performed on a Canberra S5000 High Purity Germanium (HPGe) and analyzed with the Canberra Genie 2000 software. The energy and efficiency calibration for the HPGe was performed using a mixed nuclide sealed source from Eckert and Ziegler Analytics. Radio-TLC was performed on plastic backed silica plates (ITLC-SG) purchased from Agilent Technologies (Santa Clara, CA, USA) and measured on an Eckert & Ziegler AR-2000 and processed using Winscan Radio-TLC software (Eckert and Zeigler, AR2000, Windscan softaware, Berlin, Germany). The HPLC system used for ^{43}Sc and ^{47}Sc work was an Agilent Technologies 1260 Infinity HPLC with UV and radioactivity detectors and a Xterra MS packed C18 4.6 × 150 mm column from Waters. Purity of >95% was confirmed using quantitative HPLC analysis for nonradioactive compounds and radio-TLC for radioactive compounds. Tissues weight and radioactivity was measured via an automated gamma counter (Hidex AMG, Turku, Finland). PET/CT images were acquired using a Sofie GNEXT PET/CT scanner(Sofie Biosciences, CA, USA).

3,4,3-(LI-1,2-HOPO).—The ligand was synthesized as previously described with slight modification.[24, 32, 33] Purification of the final compound was performed using HPLC. Details are presented in the Supporting Information.

Sc-HOPO.—A solution of scandium chloride ($ScCl_3 \cdot 6H_2O$) (9 mg, 34.7 μmol) in water (5 mL) was added to a solution of HOPO (25 mg, 33.3 μmol) in water (5 mL). The mixture was shaken on a thermomixer at RT for 15 minutes. The resulting solution was cloudy with white precipitate, and a pH of 3.5. A solution of 2 M K_2CO_3 was used to provide a K^+ counterion to the $Sc(HOPO)^-$ complex and to solubilize the product. At pH 7–8, the precipitate dissolved into solution with heat, and did not precipitate upon cooling. The solution was filtered, lyophilized, redissolved in water, and purified by HPLC (H_2O/ACN + 0.1 % TFA, 15–25% ACN over 15 min). NMR was performed in D_2O adjusted to pH 7 with K_2CO_3 to improve solubility. Variable pH ^{1}H NMR and ^{45}Sc NMR experiments used K_2CO_3 and DCl to adjust pH. UV-vis characterization was attempted but not conclusive. The complex was also characterized by ATR IR spectroscopy, HRMS, and X-ray crystallography. More details on these methods are presented in the Supporting Information.

Radiolabeling Studies.—^{44}Sc was received as [^{44}Sc]$ScCl_3$ in 2.0 M HCl by elution from a ^{44}Ti/^{44}Sc generator. This solution was heated to dryness and then was treated with 0.1 M HNO_3 and 30% H_2O_2 to destroy contaminants left from the elution. This was dried down and ^{44}Sc was reconstituted in 0.5 – 1.0 mL 0.1 M HCl. HOPO and DOTA were labeled at various concentrations (5 – 250 μM) in water with 100 mM ammonium acetate at pH 5. Radiolabeling times varied from 5 – 60 min. Radiolabeling experiments were carried

out at RT, 37 °C, and 95 °C with pH values ranging from 1–8. Radiolabeling reactions were performed with activity ranging from 5 μCi – 1 mCi. Reactions were monitored via radio-TLC using plastic backed silica gel TLC strips and 50 mM EDTA at pH 5 as the mobile phase. [^{44}Sc]Sc-ligand complexes move with an R_f = 0.2 while free ^{44}Sc was complexed by EDTA and moved with the solvent front.

^{43,47}Sc was produced via proton bombardment on enriched [^{46,50}Ti]TiO_2 respectively.[43] After bombardment, the [^{50}Ti]TiO_2 was dissolved using a 3:1 mass ratio of NH_4HF_2 at 250 °C and brought into solution with 5 mL concentrated HCl. The solution was diluted to 10.5 M HCl before addition to a 150 mg preconditioned branched *N,N,N',N'*-tetra-n-octyldiglcolamide resin. The column was rinsed with 9 M HCl, 7 M HNO_3 and 1 M HNO_3 before the ^{43,47}Sc was eluted in 0.1 M HCl. The collected ^{47}Sc was dried down and redissolved in 200 μL 0.25 M ammonium acetate pH 4. For HOPO, 260 μCi of ^{47}Sc was used for labeling in a 194 μL solution with .21 mM HOPO, pH 8, at 37 °C, 800 rpm for 30 minutes with an apparent molar activity of 6.4 mCi/μmol of [^{47}Sc]Sc-HOPO. For DOTA, 260 μCi of ^{47}Sc was used for labeling in a final volume of 145μL with a final concentration of 0.21 mM DOTA, pH 4 at 95 °C for 30 minutes with an apparent molar activity of 8.5 mCi/μmol of [^{47}Sc]Sc-DOTA. Radiolabeling was verified by ITLC-SG strips developed in 50 mM EDTA. Free ^{47}Sc moved with the solvent front while the labeled complex had an R_f = 0.65.

DFT Calculations

All calculations were based on Density Functional Theory (DFT) within the B3LYP approximation.[44] For the Sc atom the lanl2tz(f) basis set was used,[45] whereas all non-transition metals were represented with the 6–311G+(d,p) basis set.[46] For all systems the lowest energy structure was obtained by doing a full geometry optimization. A harmonic vibrational analysis was performed on the optimized structures to ensure that a minimum was located, and to obtain thermodynamic properties. Calculations were performed in the vapor phase and in solution using the conductor-like polarizable continuum model (CPCM) for water.[47] All calculations were performed using Gaussian 09.[48] The crystal structure obtained experimentally for the $Sc(HOPO)^{-1}$ (8-coordinate complex) was used as the initial structure in the optimization procedure. The 7-coordinate complexes were generated by adding a proton to the outer (called 7-coordinate B) or inner (called 7-coordinate C) oxygen in the hydroxypyridinonate group. The stability of the 8- and 7-coordinate complexes were computed for the following reactions:

$$HOPO^{-4} + Sc(H_2O)_6^{+3} \rightarrow Sc(HOPO)^{-1} + 6H_2O$$

Rxn 1

$$Sc(HOPO)^{-1} + H_3O^{+} \rightarrow Sc(HOPOH) + H_2O\,7-\text{coordinate A} \rightarrow Sc(HOPOH) + H_2O\,7-\text{coordinate B}$$

Rxn 2

The change in Gibbs free energy for these reactions in the vapor were obtained from:

$$\Delta G^{v}_{Rx1} = G^{v}_{Sc(HOPO)^{-1}} + 6G^{v}_{H_2O} - G^{v}_{(HOPO)^{-4}} - G^{v}_{Sc(H_2O)^{+3}} \quad (1)$$

$$\Delta G^{v}_{Rx2} = G^{v}_{Sc(HOPOH)} - G^{v}_{Sc(HOPO)^{-1}} - G^{v}_{(H_2O)^{+}} \quad (2)$$

To obtain the change in Gibbs free energy in solution, a thermodynamic cycle[49, 50] (Figure 15) was used such that

$$\Delta G^{s}_{Rx1\ or\ Rx2} = G^{v}_{Rx1\ or\ Rx2} + \sum_{i=1}^{M} \Delta G_i^{solvation} - \sum_{i=1}^{N} \Delta G_i^{solvation} \quad (3)$$

where M and N are the total number of reactant and product molecules, respectively, and $\Delta G_i^{solvation}$ is the change in Gibbs free energy of solvation of species i. A similar cycle was used to obtain changes in enthalpy in solution. The change in entropy was obtained from $\Delta S = \frac{\Delta H - \Delta G}{T}$. All thermodynamic quantities are reported at T = 300 K. Additionally, the change in electronic energy for both Rxn 1 and Rxn 2 were obtained using the DFT/B3LYP/6–311G+(d,p) energy obtained after minimization.

Stability Studies

For each stability study (EDTA challenge study or metal challenge study), a vial of 120 μCi of [^{47}Sc]Sc-DOTA or [^{47}Sc]Sc-HOPO from the stock solution was diluted to 1200 μL with Chelex water.

EDTA Challenge Study

An EDTA challenge was performed at varying pH of 5, 6, 7, and 8. Each pH challenge was done in triplicate. Each vial contained 100 μL of the stock solution of either [^{47}Sc]Sc-DOTA or [^{47}Sc]Sc-HOPO for an average of 10μCi. 50 μL of EDTA was added to solution and diluted to 500 μL with Chelex purified water for a final concentration of 10 μM ligand and 100 μM EDTA. Solutions were assessed via ITLC at 15 minutes, 30 minutes, 1 hour, and then daily time points up to 7 days. Solutions were kept at 37 °C with agitation throughout this study.

Metal Challenge Study

A metal challenge was performed with $FeCl_2$, $CuCl_2$, $MgCl_2$ and $ZnCl_2$ in triplicate. Each vial contained 100 μL of the stock solution of either [^{47}Sc]Sc-DOTA or [^{47}Sc]Sc-HOPO for an average of 10 μCi. 50 μL of the metal solution was added to solution and then diluted to 500 μL with Chelex purified water for a final concentration of 10 μM ligand and 100 μM

metal. Solutions were assessed via ITLC at 15 minutes, 30 minutes, 1 hour, and then daily time points up to 7 days. Solutions were kept at 37 °C with agitation throughout this study.

PET Imaging and Biodistribution

HOPO was radiolabeled with either ^{43}Sc or ^{47}Sc in yields >96%, at 37 °C at pH 8 for 30 minutes as described above. The dose was diluted with 0.9% NaCl solution to achieve 100 μL injections: 10 μCi injections of [^{47}Sc]Sc-HOPO (apparent molar activity of 8.4 mCi/μmol for stock dose) and 100 μCi of [^{43}Sc]Sc-HOPO (apparent molar activity of 12.4 mCi/μmol for stock dose). The radiolabeled doses did not require purification prior to injection. Longer term biodistributions were analyzed with the [^{47}Sc]Sc-HOPO for four time points: 10 minutes, 1 hour, 4 hours, and 24 hours. At each time point mice (n=4) were sacrificed and radioactivity assessed in the following organs: 50 μL of blood, heart, lung, liver, spleen, pancreas stomach, kidneys, small intestine, large intestine, fat, skin, muscle, femur, brain, and tail. Each sample was added to a pre-weighed vial. The vials were weighed, counted on a gamma counter, and the percentage of injected dose per gram tissue was calculated.

PET (energy window 350–650 keV) and CT (voltage 80 kVp, current 150 μA, 720 projections, scan time 5 minutes) imaging was performed immediately after retro orbital injection of 100 μCi of [^{43}Sc]Sc-HOPO. PET data was collected for 90-minute dynamic imaging, followed by 5-minute CT. Following imaging, biodistribution was conducted as described above. PET images were reconstructed via 3D-OSEM(Ordered Subset Expectation Maximization) algorithm (24 subsets and 3 iterations), with random, attenuation, and decay correction and CT was reconstructed with Modified Feldkamp Algorithm, and analyzed using VivoQuant (VivoQuant 4.0, Invicro Imaging Service and Software, Boston USA) software. After images were reconstructed, the PET images were appended to the CT. Following image reconstruction, regions of interest were drawn for select tissues (brain, lung, liver, kidney, and muscle) in each mouse based on the CT images for each frame. The time-activity curves (TAC) of the uptake of the tracer were generated over the course of the data collection.

Supplementary Material

Refer to Web version on PubMed Central for supplementary material.

Acknowledgements

The authors would like to thank the Medical Isotopes Research and Production (MIRP) Group at Brookhaven National Laboratory for providing the ^{44}Sc used in this paper through the support of DOE IP# ST5001020 (CSC). The authors also acknowledge the NSF-IGERT Program NSF-DGE 0965983 (LCF), and The Tow Foundation Graduate Fellowship from the MSKCC Center for Molecular Imaging and Nanotechnology (MDP) and CUNY Hunter College for their support of this research. The authors also thank Hunter Mass Spectrometry. Research reported in this publication was supported by the National Institute of General Medical Sciences of the National Institutes of Health under Award Number SC2GM130464 (MAD). The content is solely the responsibility of the authors and does not necessarily represent the official views of the National Institutes of Health. The MSK Radiochemistry and Molecular Imaging Probes Core Facility and the MSK Small Animal Imaging Facility were supported in part by NIH P30 CA08748. This study was also supported in part by NIH R35 CA232130-01A1 (JSL). The production of ^{43}Sc and ^{47}Sc was supported by the Department of Energy Isotope Program under DESC0020197 (SEL). Small animal imaging studies were supported by the O'Neal Comprehensive Cancer Center at UAB through P30CA013148.

References

1. . FDA-approved radiopharmaceuticals 2022. https://www.cardinalhealth.com/content/dam/corp/web/documents/fact-sheet/cardinal-health-fda-approved-radiopharmaceuticals.pdf (accessed 10/19/2022).
2. information extracted from the NuDat database. National Nuclear Data Center: 2021.
3. Müller C; Bunka M; Haller S; Köster U; Groehn V; Bernhardt P; van der Meulen N; Türler A; Schibli R, Promising Prospects for 44Sc-/47Sc-Based Theragnostics: Application of 47Sc for Radionuclide Tumor Therapy in Mice. J. Nuc. Med 2014, 55 (10), 1658–1664.
4. Kerdjoudj R; Pniok M; Alliot C; Kubicek V; Havlickova J; Rosch F; Hermann P; Huclier-Markai S, Scandium(iii) complexes of monophosphorus acid DOTA analogues: a thermodynamic and radiolabelling study with 44Sc from cyclotron and from a 44Ti/44Sc generator. Dalton Trans. 2016, 45 (4), 1398–1409. [PubMed: 26675416]
5. Domnanich KA; Müller C; Farkas R; Schmid RM; Ponsard B; Schibli R; Türler A; van der Meulen NP, (44)Sc for labeling of DOTA- and NODAGA-functionalized peptides: preclinical in vitro and in vivo investigations. EJNMMI radiopharmacy and chemistry 2017, 1 (1), 8–8. [PubMed: 29564385]
6. Eppard E; de la Fuente A; Benešová M; Khawar A; Bundschuh RA; Gärtner FC; Kreppel B; Kopka K; Essler M; Rösch F, Clinical Translation and First In-Human Use of [(44)Sc]Sc-PSMA-617 for PET Imaging of Metastasized Castrate-Resistant Prostate Cancer. Theranostics 2017, 7 (18), 4359–4369. [PubMed: 29158832]
7. Umbricht CA; Benesova M; Schmid RM; Turler A; Schibli R; van der Meulen NP; Muller C, (44)Sc-PSMA-617 for radiotheragnostics in tandem with (177)Lu-PSMA-617-preclinical investigations in comparison with (68)Ga-PSMA-11 and (68)Ga-PSMA-617. EJNMMI Res 2017, 7 (1), 9. [PubMed: 28102507]
8. Edem PE; Sinnes JP; Pektor S; Bausbacher N; Rossin R; Yazdani A; Miederer M; Kjaer A; Valliant JF; Robillard MS; Rosch F; Herth MM, Evaluation of the inverse electron demand Diels-Alder reaction in rats using a scandium-44-labelled tetrazine for pretargeted PET imaging. Ejnmmi Research 2019, 9.
9. Siwowska K; Guzik P; Domnanich KA; Monné Rodríguez JM; Bernhardt P; Ponsard B; Hasler R; Borgna F; Schibli R; Köster U; van der Meulen NP; Müller C, Therapeutic Potential of (47)Sc in Comparison to (177)Lu and (90)Y: Preclinical Investigations. Pharmaceutics 2019, 11 (8), 424. [PubMed: 31434360]
10. Hernandez R; Valdovinos HF; Yang Y; Chakravarty R; Hong H; Barnhart TE; Cai W, 44Sc: An Attractive Isotope for Peptide-Based PET Imaging. Mol. Pharm 2014, 11 (8), 2954–2961. [PubMed: 25054618]
11. Honarvar H; Müller C; Cohrs S; Haller S; Westerlund K; Karlström AE; van der Meulen NP; Schibli R; Tolmachev VM, Evaluation of the first 44Sc-labeled Affibody molecule for imaging of HER2-expressing tumors. Nuclear medicine and biology 2017, 45, 15–21. [PubMed: 27837664]
12. Price EW; Orvig C, Matching chelators to radiometals for radiopharmaceuticals. Chem. Soc. Rev 2014, 43 (1), 260–90. [PubMed: 24173525]
13. Zeglis BM; Houghton JL; Evans MJ; Viola-Villegas N; Lewis JS, Underscoring the influence of inorganic chemistry on nuclear imaging with radiometals. Inorg. Chem 2014, 53 (4), 1880–99. [PubMed: 24313747]
14. Walczak R; Gawęda W; Dudek J; Choiński J; Bilewicz A, Influence of metal ions on the 44Sc-labeling of DOTATATE. J. Radioanal. Nucl. Chem 2019, 322 (2), 249–254.
15. Eppard E; De la Fuente A; Benesova M; Khawar A; Bundschuh RA; Gartner FC; Kreppel B; Kopka K; Essler M; Rosch F, Clinical Translation and First In-Human Use of [44Sc]Sc-PSMA-617 for PET Imaging of Metastasized Castrate-Resistant Prostate Cancer. Theranostics 2017.
16. Połosak M; Piotrowska A; Krajewski S; Bilewicz A, Stability of 47Sc-complexes with acyclic polyamino-polycarboxylate ligands. J. Radioanal. Nucl. Chem 2013, 295 (3), 1867–1872. [PubMed: 26224932]

17. Huclier-Markai S; Alliot C; Sebti J; Brunel B; Aupiais J, A comparative thermodynamic study of the formation of scandium complexes with DTPA and DOTA. RSC Advances 2015, 5 (121), 99606–99617.

18. Huclier-Markai S; Sabatie A; Ribet S; Kubicek V; Paris M; Vidaud C; Hermann P; Cutler CS, Chemical and biological evaluation of scandium(III)-polyaminopolycarboxylate complexes as potential PET agents and radiopharmaceuticals. Radiochimica Acta 2011, 99 (10), 653–662.

19. Sinnes JP; Nagel J; Rosch F, AAZTA(5)/AAZTA(5)-TOC: synthesis and radiochemical evaluation with (68)Ga, (44)Sc and (177)Lu. EJNMMI Radiopharm Chem 2019, 4 (1), 18. [PubMed: 31659525]

20. Vaughn BA; Ahn SH; Aluicio-Sarduy E; Devaraj J; Olson AP; Engle J; Boros E, Chelation with a twist: a bifunctional chelator to enable room temperature radiolabeling and targeted PET imaging with scandium-44. Chemical Science 2020, 11 (2), 333–342. [PubMed: 32953004]

21. Chakravarty R; Goel S; Valdovinos HF; Hernandez R; Hong H; Nickles RJ; Cai W, Matching the decay half-life with the biological half-life: ImmunoPET imaging with (44)Sc-labeled cetuximab Fab fragment. Bioconjug Chem 2014, 25 (12), 2197–204. [PubMed: 25389697]

22. Daumann LJ; Tatum DS; Snyder BER; Ni C; Ga-lai L; Solomon EI; Raymond KN, New Insights into Structure and Luminescence of EuIII and SmIII Complexes of the 3,4,3-LI(1,2-HOPO) Ligand. Journal of the American Chemical Society 2015, 137, 2816–2819. [PubMed: 25607882]

23. Deri MA; Ponnala S; Kozlowski P; Burton-Pye BP; Cicek HT; Hu C; Lewis JS; Francesconi LC, p-SCN-Bn-HOPO: A Superior Bifunctional Chelator for 89Zr ImmunoPET. Bioconjugate Chemistry 2015, 26 (12), 2579–2591. [PubMed: 26550847]

24. Deri MA; Ponnala S; Zeglis BM; Pohl G; Dannenberg JJ; Lewis JS; Francesconi LC, Alternative Chelator for 89Zr Radiopharmaceuticals: Radiolabeling and Evaluation of 3,4,3-(LI-1,2-HOPO). J. Med. Chem 2014, 57 (11), 4849–4860. [PubMed: 24814511]

25. An DD; Kullgren B; Jarvis EE; Abergel RJ, From early prophylaxis to delayed treatment: Establishing the plutonium decorporation activity window of hydroxypyridinonate chelating agents. Chemico-Biological Interactions 2017, 267, 80–88. [PubMed: 27038878]

26. Deblonde GJ-P; Ricano A; Abergel RJ, Ultra-selective ligand-driven separation of strategic actinides. Nature Communications 2019, 10 (2438), 1–9.

27. Migliorati V; D'Angelo P, Unraveling the Sc3+ Hydration Geometry: The Strange Case of the Far-Coordinated Water Molecule. Inorg. Chem 2016, 55 (13), 6703–6711. [PubMed: 27300102]

28. Sears JM; Boyle TJ, Structural properties of scandium inorganic salts. Coord. Chem. Rev 2017, 340, 154–171.

29. Gao S-M; Guo W-P; Ding Y-H, Maximum Carbonyl-Coordination Number of Scandium Computational Study of Sc(CO)n (n 5 1–7), Sc(CO)7 - and Sc(CO)6 3-. Int. J. Quantum Chem 2013, 113, 1192–1199.

30. Bhupathiraju NVSDK; Younes A; Cao M; Ali J; Cicek HT; Tully KM; Ponnala S; Babich JW; Deri MA; Lewis JS; Francesconi LC; Drain CM, Improved synthesis of the bifunctional chelator p-SCN-Bn-HOPO. Organic & Biomolecular Chemistry 2019, 17 (28), 6866–6871. [PubMed: 31268109]

31. Shannon RD, Revised Effective Ionic Radii and Systematic Studies of Interatomie Distances in Halides and Chaleogenides. Acta Crystallogr. Sect. A: Found. Crystallogr 1976, 32, 751–767.

32. Xu J; Durbin PW; Kullgren B; Ebbe SN; Uhlir LC; Raymond KN, Synthesis and Initial Evaluation for In Vivo Chelation of Pu(IV) of a Mixed Octadentate Spermine-Based Ligand Containing 4-Carbamoyl-3-hydroxy-1-methyl-2(1H)-pyridinone and 6-Carbamoyl-1-hydroxy-2(1H)-pyridinone. J. Med. Chem 2002, 45 (18), 3963–3971. [PubMed: 12190318]

33. Fritsch P; Herbreteau D; Moutairou K; Lantenois G; Richard-le Naour H; Grillon G; Hoffschir D; Poncy JL; Laurent A; Masse R, Comparative Toxicity of 3,4,3-LIHOPO and DTPA in Baboons: Preliminary Results. Radiation Protection Dosimetry 1994, 53 (1–4), 315–318.

34. Abergel RJ; Durbin PW; Kullgren B; Ebbe SN; Xu J; Chang PY; Bunin DI; Blakely EA; Bjornstad KA; Rosen CJ; Shuh DK; Raymond KN, Biomimetic actinide chelators: an update on the preclinical development of the orally active hydroxypyridonate decorporation agents 3,4,3-LI(1,2-HOPO) and 5-LIO(Me-3,2-HOPO). Health Phys. 2010, 99 (3), 401–7. [PubMed: 20699704]

35. Pniok M; Kubíček V; Havlíčková J; Kotek J; Sabatie-Gogová A; Plutnar J; Huclier-Markai S; Hermann P, Thermodynamic and Kinetic Study of Scandium(III) Complexes of DTPA and DOTA: A Step Toward Scandium Radiopharmaceuticals. Chemistry – A European Journal 2014, 20 (26), 7944–7955. [PubMed: 24838869]
36. Nagy G; Szikra D; Trencsényi G; Fekete A; Garai I; Giani AM; Negri R; Masciocchi N; Maiocchi A; Uggeri F; Tóth I; Aime S; Giovenzana GB; Baranyai Z, AAZTA: An Ideal Chelating Agent for the Development of 44Sc PET Imaging Agents. Angew. Chem. Int. Ed 2017, 56 (8), 2118–2122.
37. Rehder D; Speh M, An exploratory scandium-45 NMR study into the complexation of alanine and oligopeptides. Inorg. Chim. Acta 1987, 135 (1), 73–79.
38. Rehder D; Hink K, The interaction of Sc(OH)2+·aq with serine and small peptides investigated by 45Sc NMR spectroscopy. Inorg. Chim. Acta 1989, 158 (2), 265–271.
39. Nonat AM; Gateau C; Fries PH; Helm L; Mazzanti M, New Bisaqua Picolinate-Based Gadolinium Complexes as MRI Contrast Agents with Substantial High-Field Relaxivities. Eur. J. Inorg. Chem 2012, 2012 (12), 2049–2061.
40. Carter KP; Deblonde GJP; Lohrey TD; Bailey TA; An DD; Shield KM; Lukens WW; Abergel RJ, Developing scandium and yttrium coordination chemistry to advance theranostic radiopharmaceuticals. Communications Chemistry 2020, 3 (1), 61. [PubMed: 36703424]
41. Aihara J. i., Reduced HOMO−LUMO Gap as an Index of Kinetic Stability for Polycyclic Aromatic Hydrocarbons. The Journal of Physical Chemistry A 1999, 103 (37), 7487–7495.
42. Miar M; Shiroudi A; Pourshamsian K; Oliaey A; Hatamjafari F, Theoretical investigations on the HOMO–LUMO gap and global reactivity descriptor studies, natural bond orbital, and nucleus-independent chemical shifts analyses of 3-phenylbenzo[d]thiazole-2(3 H)-imine and its para -substituted derivatives: Solvent and substituent effects. Journal of Chemical Research 2020, 45, 174751982093209.
43. Loveless CS; Blanco JR; Diehl GL; Elbahrawi RT; Carzaniga TS; Braccini S; Lapi SE, Cyclotron Production and Separation of Scandium Radionuclides from Natural Titanium Metal and Titanium Dioxide Targets. J. Nuc. Med 2021, 62 (1), 131.
44. Becke AD, A new mixing of Hartree–Fock and local density-functional theories. The Journal of Chemical Physics 1993, 98 (2), 1372–1377.
45. Roy LE; Hay PJ; Martin RL, Revised Basis Sets for the LANL Effective Core Potentials. Journal of Chemical Theory and Computation 2008, 4 (7), 1029–1031. [PubMed: 26636355]
46. Hehre WJ; Ditchfield R; Pople JA, Self—Consistent Molecular Orbital Methods. XII. Further Extensions of Gaussian—Type Basis Sets for Use in Molecular Orbital Studies of Organic Molecules. The Journal of Chemical Physics 1972, 56 (5), 2257–2261.
47. Cossi M; Rega N; Scalmani G; Barone V, Energies, structures, and electronic properties of molecules in solution with the C-PCM solvation model. J. Comput. Chem 2003, 24 (6), 669–681. [PubMed: 12666158]
48. Frisch MJ, G. W. T., Schlegel HB, Scuseria GE, Robb MA, Cheeseman Scalmani G, Barone V, Peterrson GA, Nakatsuji H, Li X, Caricato M, Marenich A, Bloino J, Janesko BG, Gomperts R, Mennucci B, Hratchian HP, Ortiz JV, Izmaylov AF, Sonnenberg JL, Williams-Young D, Ding F, Lipparini F, Egidi F, Goings J, Peng B, Petrone A, Henderson T, Ranasinghe D, Zakrzewski VG, Gao J, Rega N, Zheng G, Liang W, Hada M, Ehara M, Toyota K, Fukuda R, Hasegawa J, Ishida M, Nakajima T, Honda Y, Kitao O, Nakai T, Vreven T, Throssell K, Montgomery JA Jr., Peralta JE, Ogliaro F, Bearpark M, Heyd JJ, Brothers E, Kudin KN, Staroverov VN, Keith T, Kobayashi R, Normand J, Raghavarachi K, Rendell A, Burant JC, Iyengar SS, Tomasi J, Cossi M, Millam JM, Klene M, Adamo C, Cammi R, Ochterski JW, Martin RL, Morokuma K, Farkas O, Foresman JB, Fox DJ, Gaussian 09, Gaussian Inc: Wallingford, CT, 2016.
49. da Silva EF; Svendsen HF; Merz KM, Explicitly Representing the Solvation Shell in Continuum Solvent Calculations. The Journal of Physical Chemistry A 2009, 113 (22), 6404–6409. [PubMed: 19425558]
50. Gupta M; da Silva EF; Svendsen HF, Modeling Temperature Dependency of Amine Basicity Using PCM and SM8T Implicit Solvation Models. The Journal of Physical Chemistry B 2012, 116 (6), 1865–1875. [PubMed: 22251398]

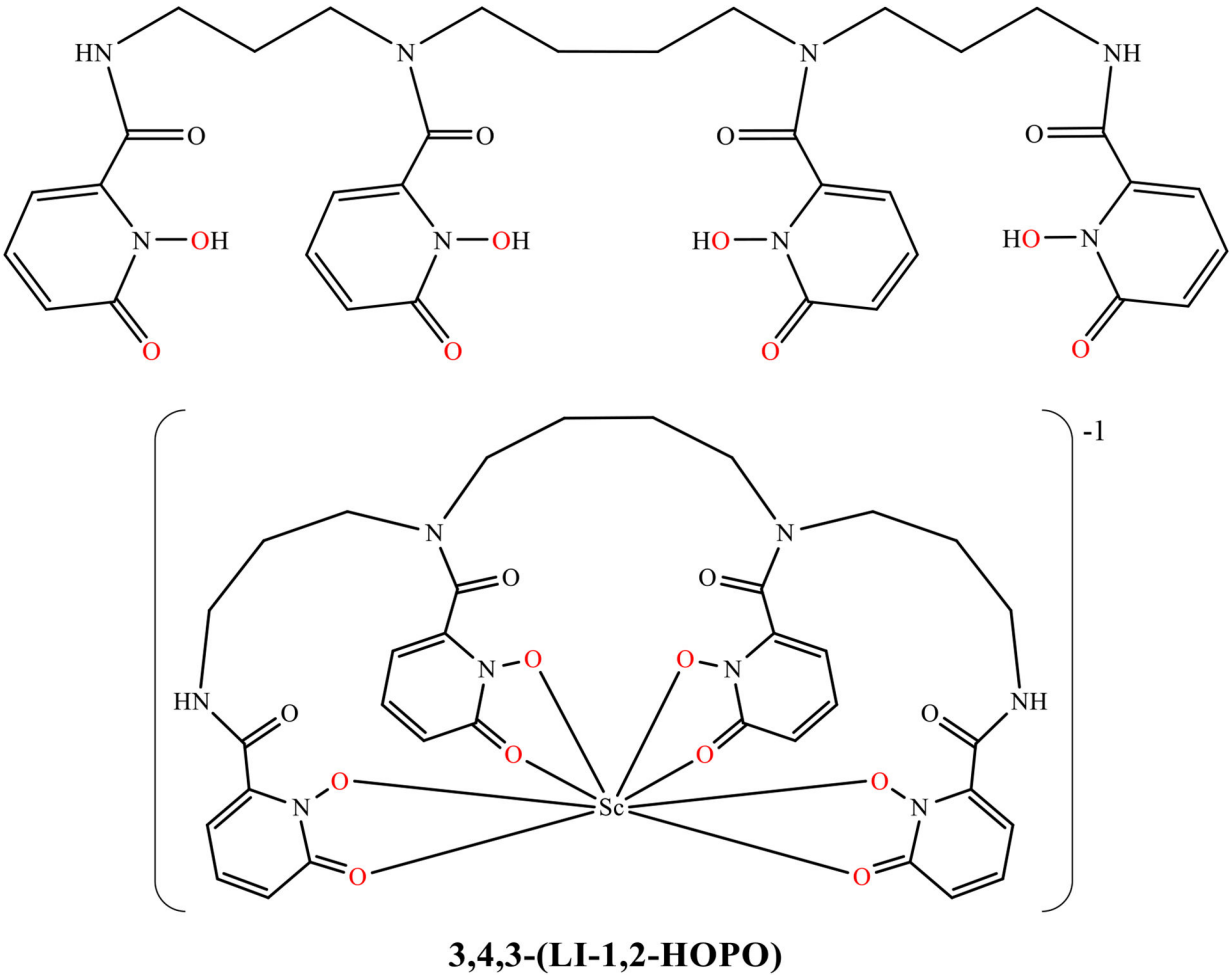

Figure 1.
Structural scheme for the HOPO ligand and the Sc-HOPO complex with the coordinating oxygen atoms shown in red.

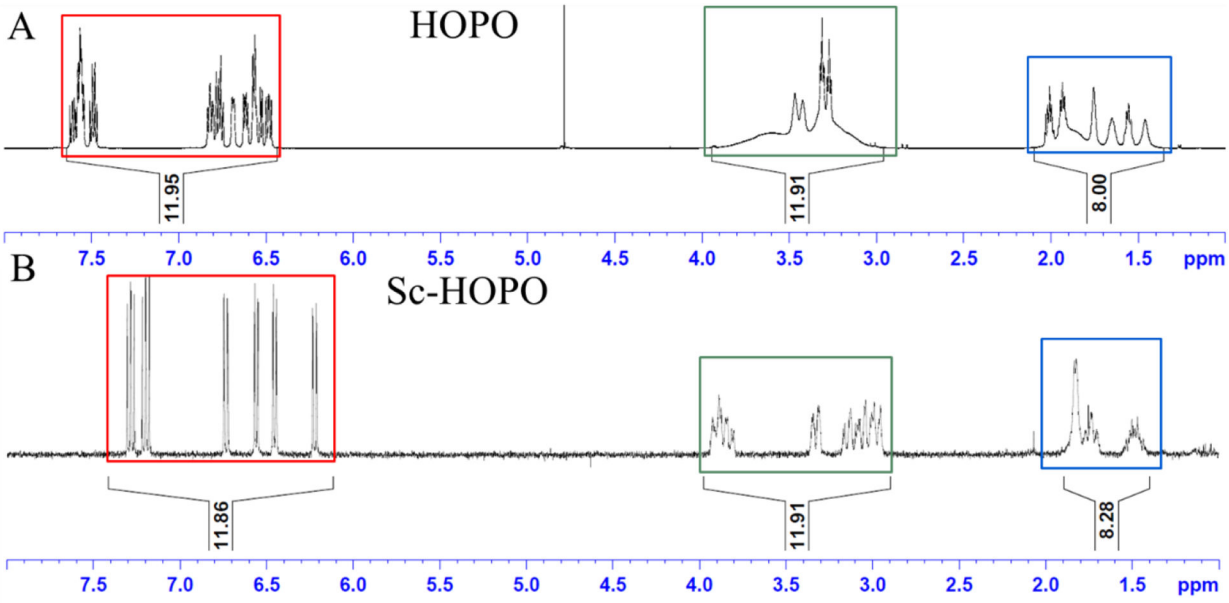

Figure 2.

^{1}H NMR of HOPO and K[Sc(HOPO)] in D_2O. Corresponding integral regions are highlighted by color.

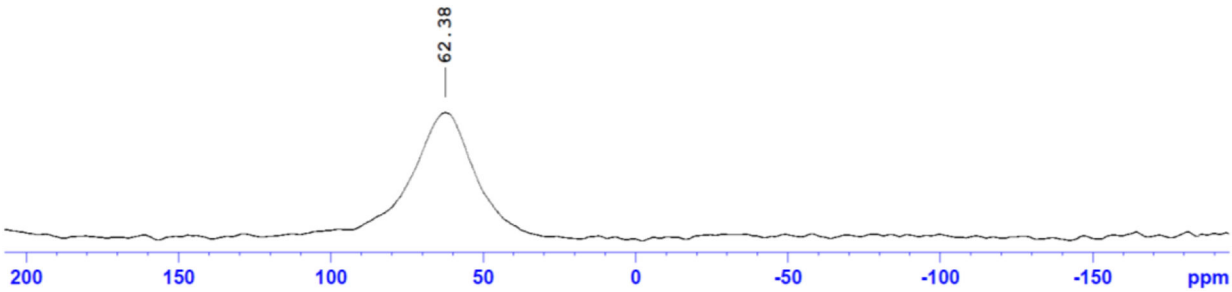

Figure 3.

^{45}Sc NMR of K[Sc(HOPO)] in D_2O. The broad peak (FWHM = 12414 Hz) is consistent with ^{45}Sc NMR of other Sc chelates. 0.1 M $ScCl_3$ in 0.01 M HCl was used as the reference standard for the NMR method.

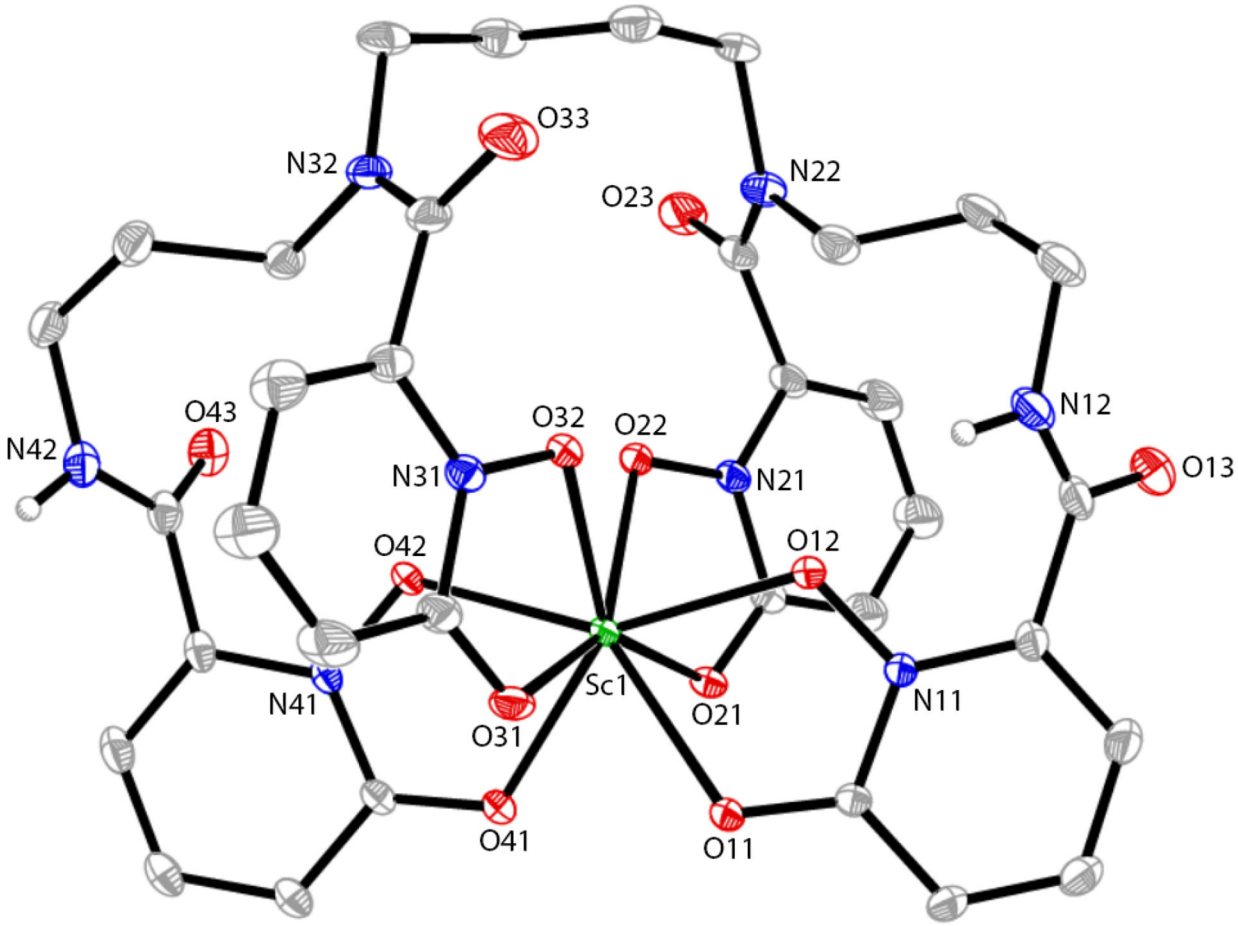

Figure 4.

Molecular diagram of the Sc-HOPO anion. Hydrogen atoms bound to carbon as well as disordered carbon atoms in the HOPO backbone are omitted for clarity. Atomic displacement parameters are displayed at the 30% probability level.

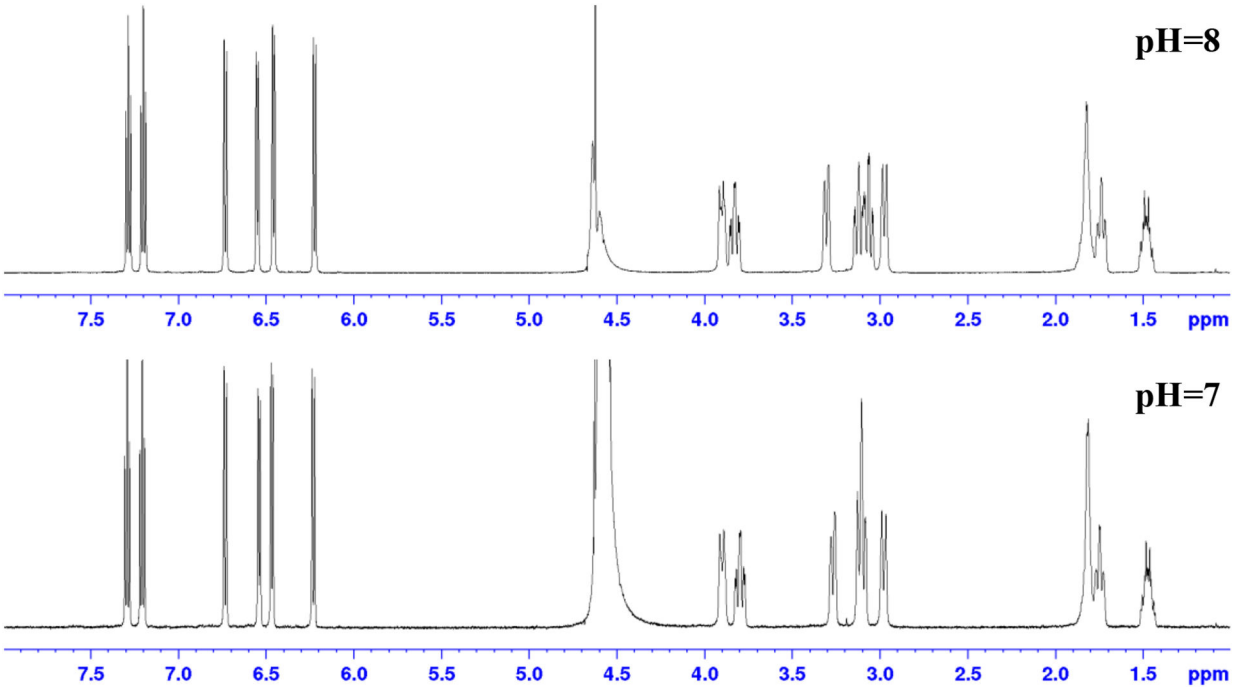

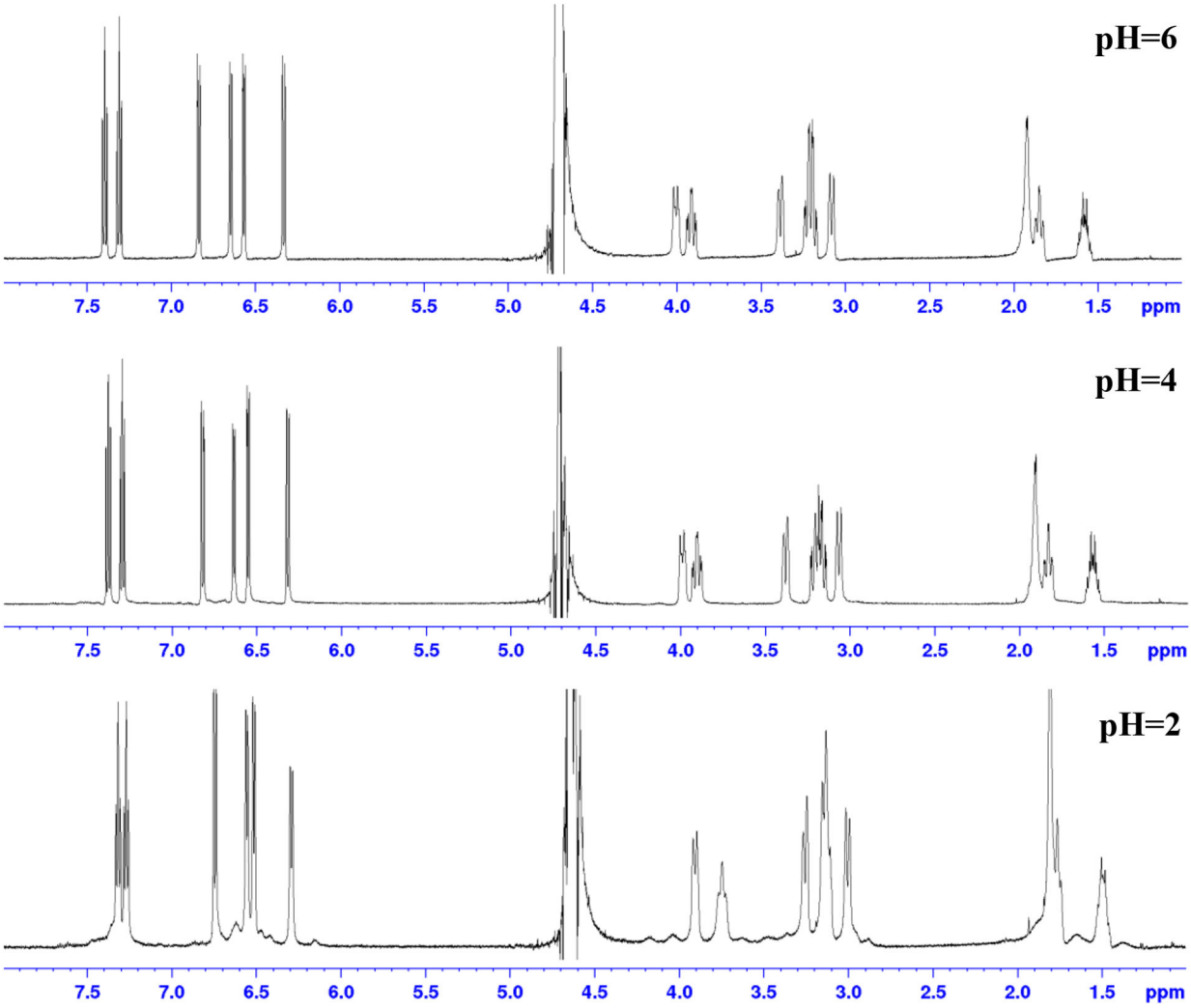

Figure 5.

^{1}H NMR of K[Sc(HOPO)] taken at different pH's in D_2O. pH was measured by pH probe, which introduced H_2O to the sample. Although peak suppression for H_2O was used in the NMR method, the quantity of water was too great for it to be effective. pH was adjusted with K_2CO_3 and DCl. The resultant increase of KCl concentration results in minor chemical shift changes for both the analyte and the solvent peak.

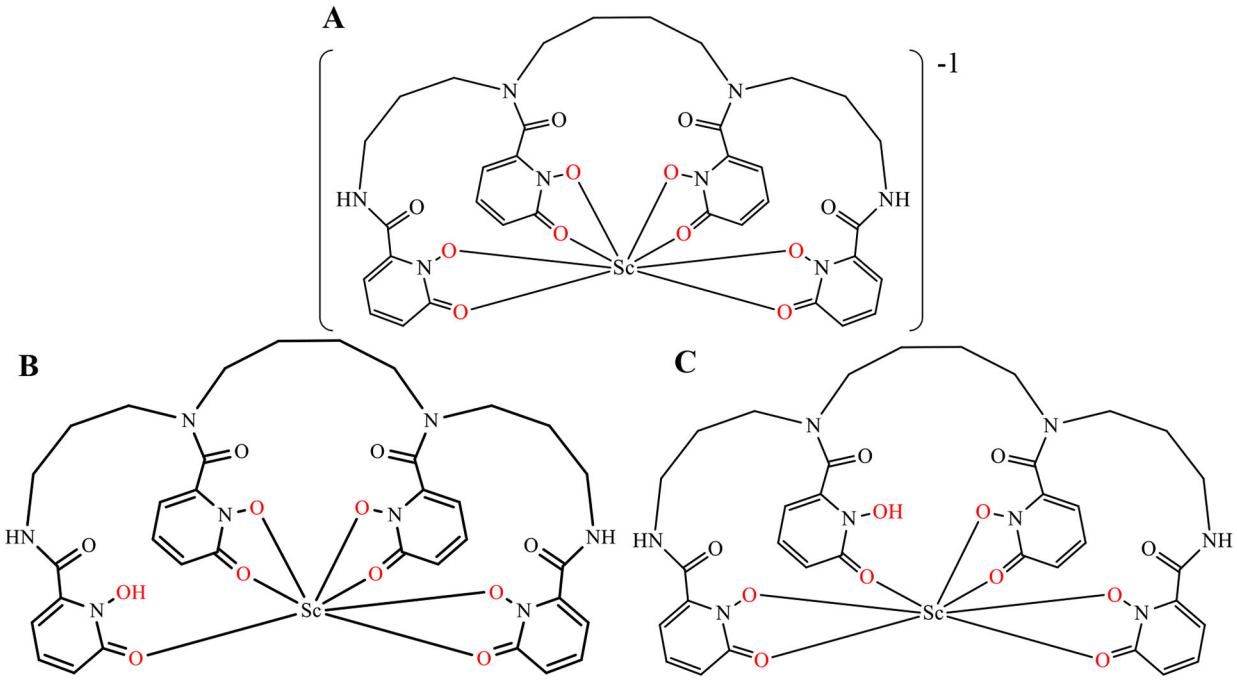

Figure 6.

8-coordinate structural scheme of Sc-HOPO (A) and alternative 7-coordinate schemes for Sc-HOPOH in low pH conditions (B and C).

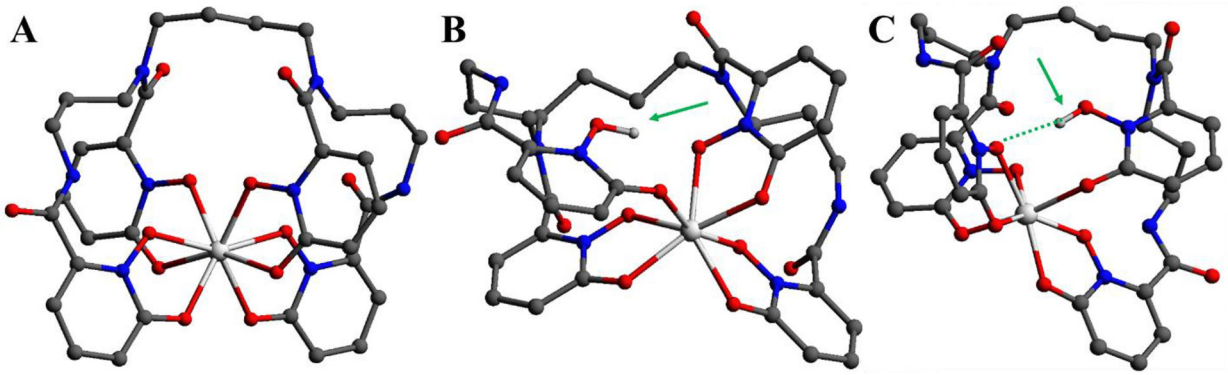

Figure 7.

Optimized equilibrium structures for: A) 8-coordinate complex, B) 7-coordinate structure with outer group protonation, and C) 7-coordinate complex with inner group protonation. All hydrogens are omitted except for the protonated OH's in complexes B and C, which are designated by green arrows. A dashed line indicates hydrogen bonding.

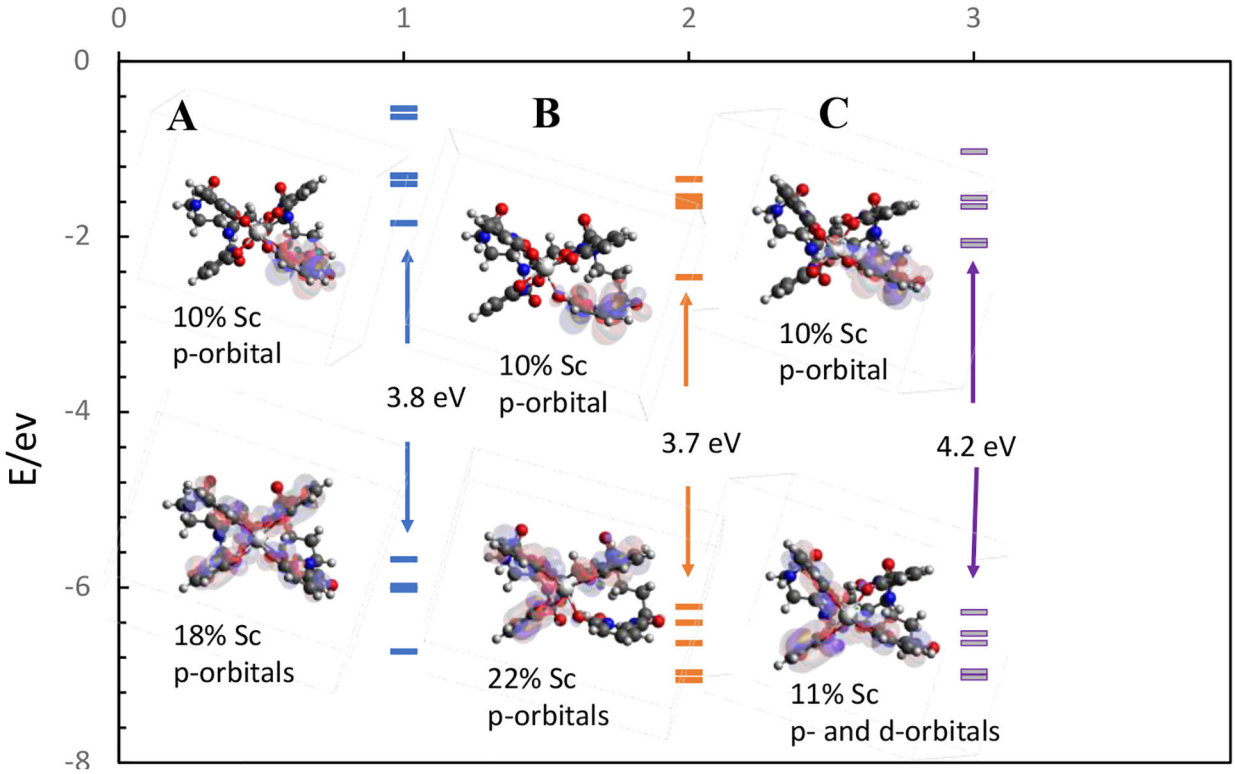

Figure 8.

The five lowest occupied and five highest unoccupied molecular orbitals energies for the 8-coordinate A (1 in the x-axis) complex, 7-coordinate B (2 in the x-axis) and 7-coordinate C (3 in the x-axis) complexes. Frontier orbital representations for the LUMO and HOMO for each complex are shown.

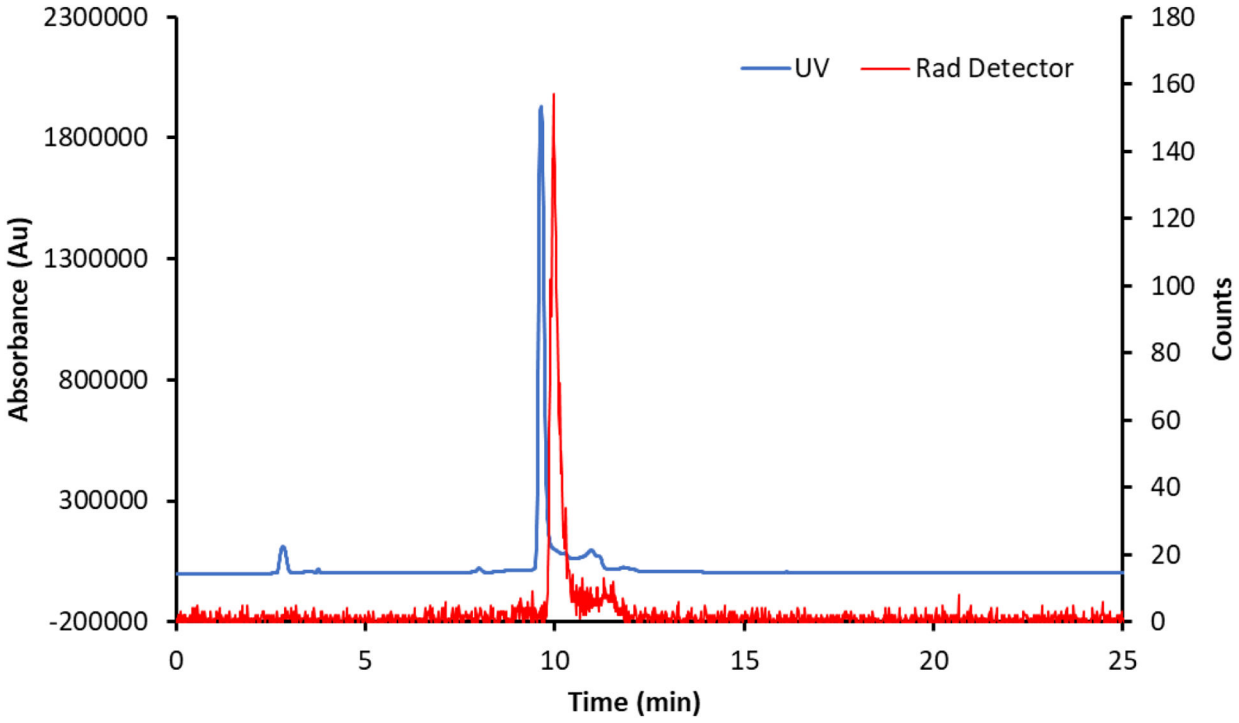

Figure 9.

Coelution of [^{47}Sc]Sc-HOPO with macroscopic, characterized Sc-HOPO. As discussed above, both macroscopic and tracer levels show tailing caused by Sc-HOPOH.

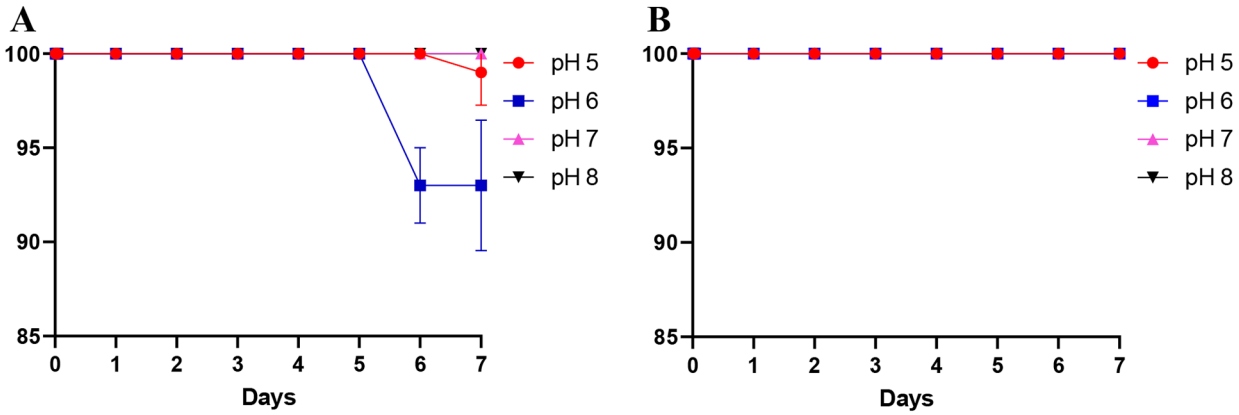

Figure 10.

Stability study of [^{47}Sc]Sc-HOPO over the course of 7 days in the presence of 100 μM of EDTA at varying pH (A). Stability of [^{47}Sc]Sc-DOTA in the presence of 100 μM EDTA at varying pH (B).

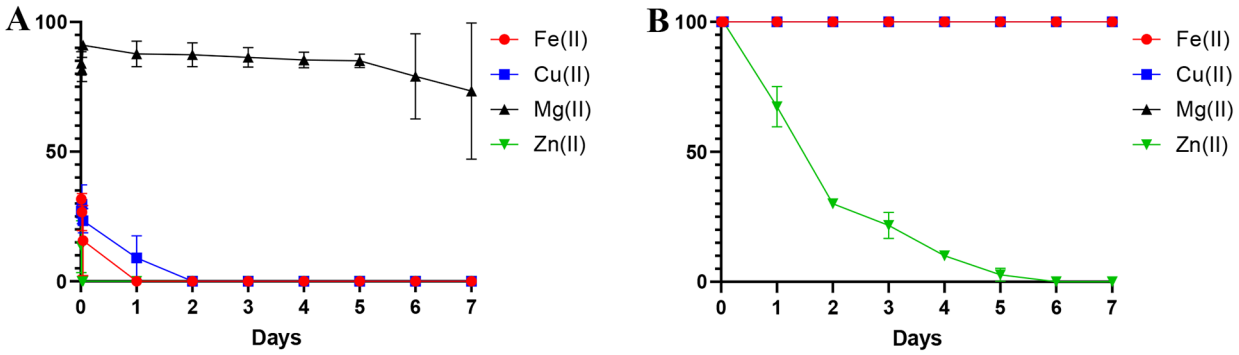

Figure 11.

Stability study of [^{47}Sc]Sc-HOPO and [^{47}Sc]Sc-DOTA over the course of 7 days in the presence of metal ions. (A) [^{47}Sc]Sc-HOPO in the presence of 100 μM of $FeCl_2$, $CuCl_2$. $MgCl_2$ and $ZnCl_2$. (B) Stability of [^{47}Sc]Sc-DOTA in the presence of 100 μM of $FeCl_2$, $CuCl_2$. $MgCl_2$ and $ZnCl_2$.

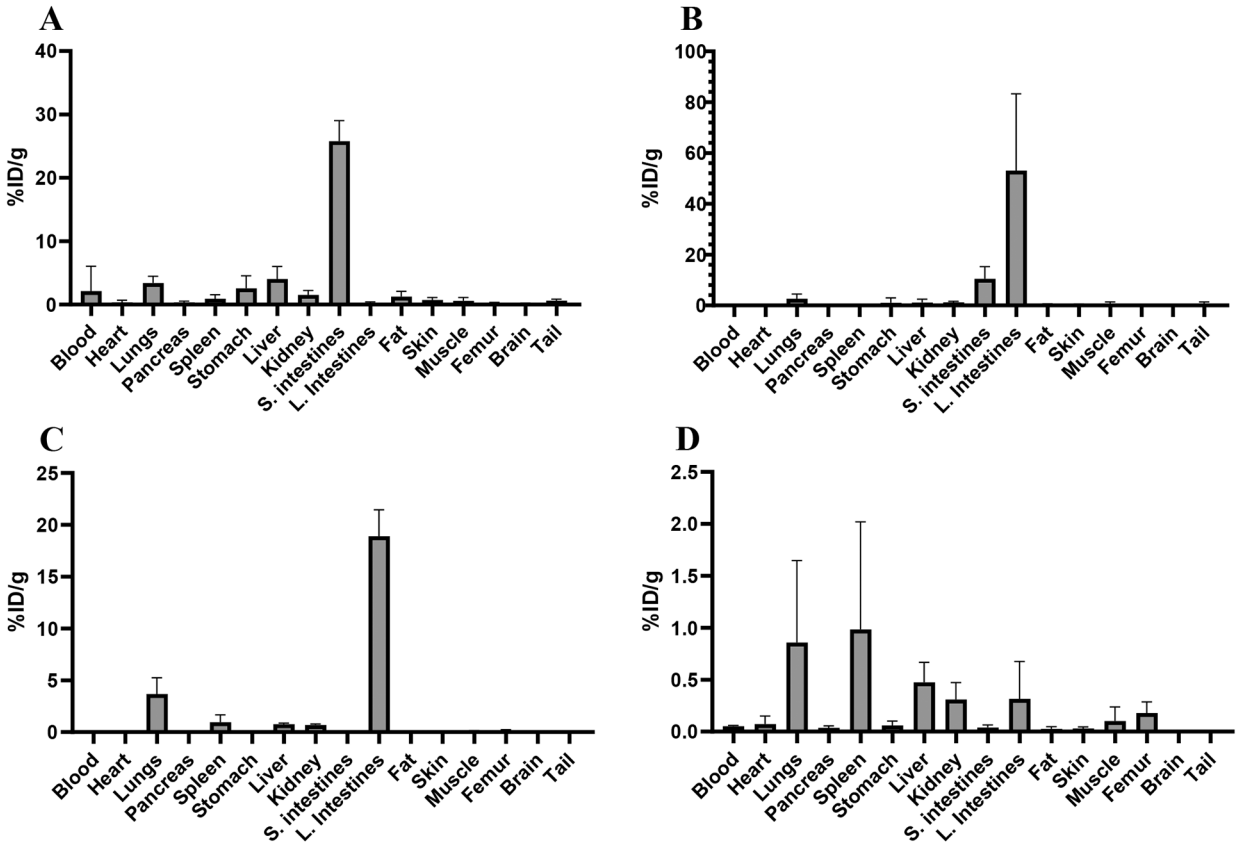

Figure 12.

Biodistribution of 10 μCi injections of [^{47}Sc]Sc-HOPO in female Balb/c mice at four time points: 10 minutes (A), 1 hour (B), 4 hours (C) and 24 hours (D).

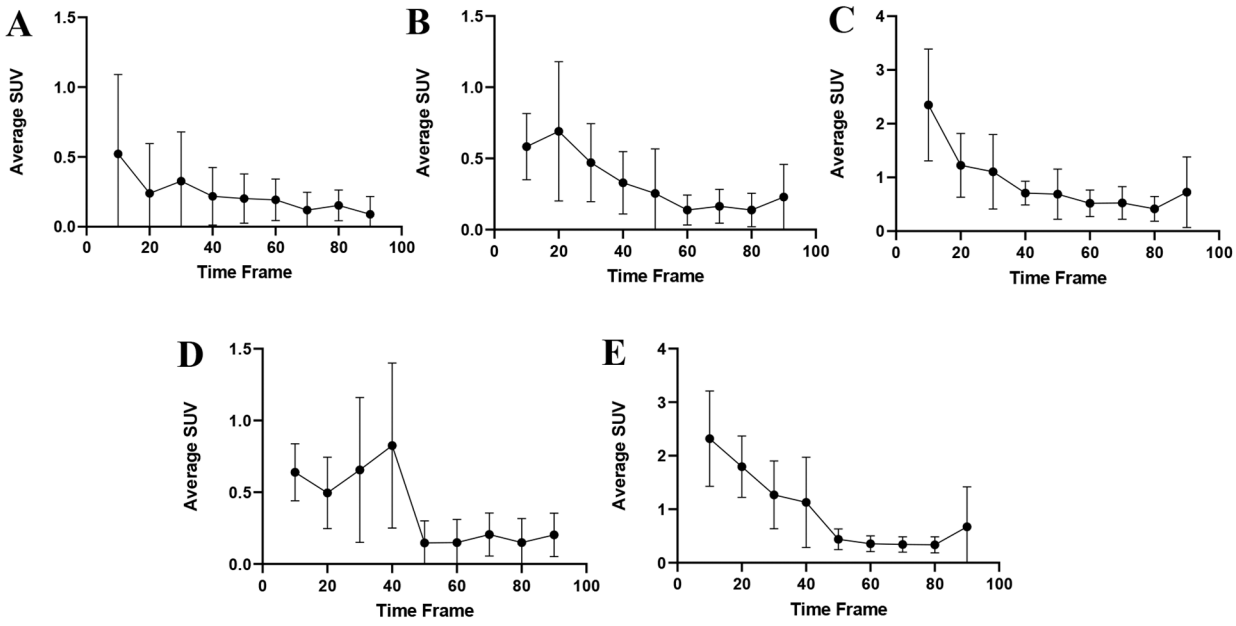

Figure 13:

The standard uptake values for various organs of 100 μCi of [^{43}Sc]Sc-HOPO were taken at 10 minute intervals over the course of the 90 minute scan and each organ was then plotted to create a time activity curve for each organ: Brain (A), Lung (B), Kidney (C), Heart (D) and Liver (E).

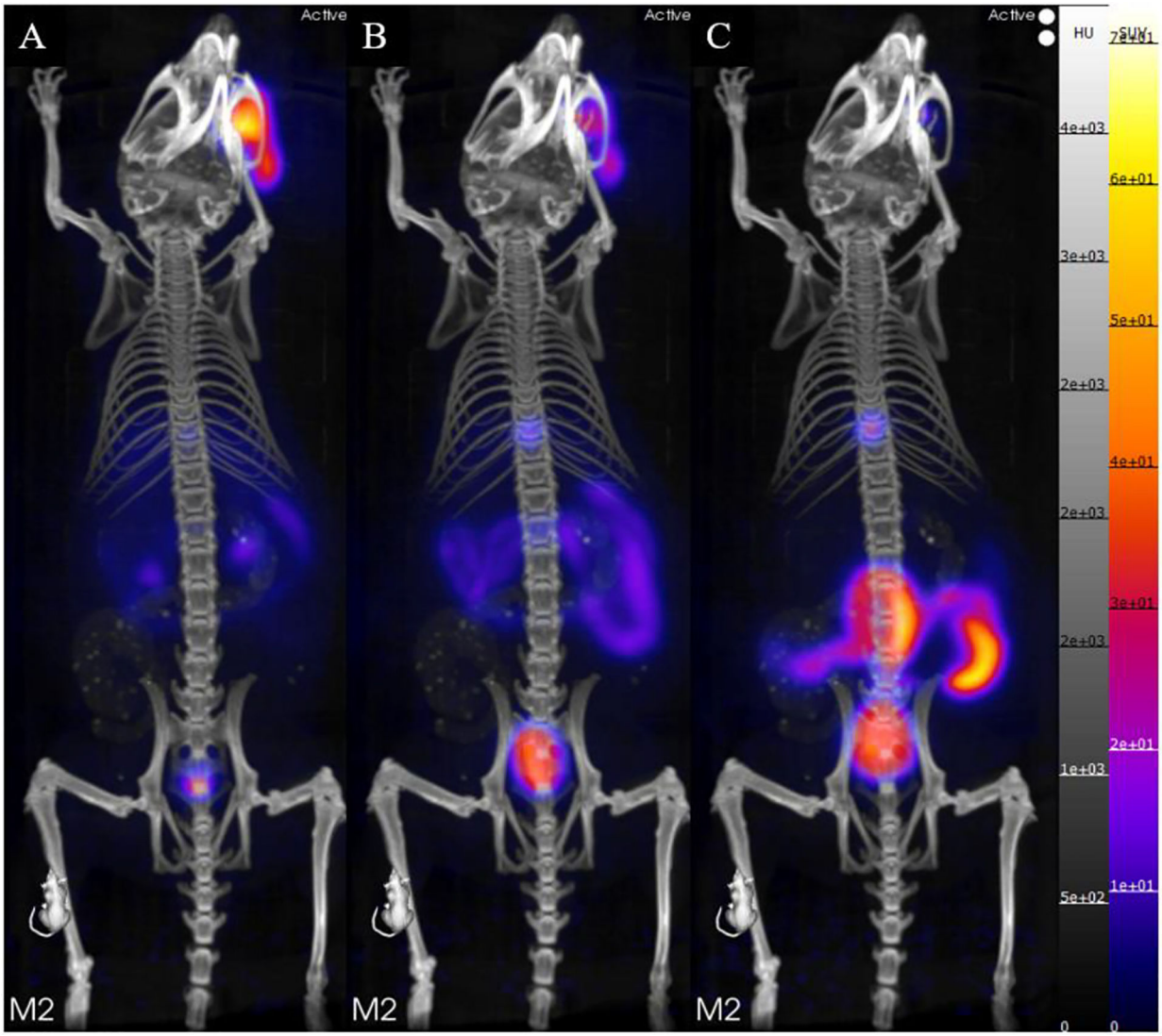

Figure 14.

(A) PET/CT static image of a Balb/c mouse 0–10 minutes after injection of [^{43}Sc]Sc-HOPO. (B) PET/CT static image of a Balb/c mouse 4–50 minutes after injection of [^{43}Sc]Sc-HOPO. (C) PET/CT static image of a Balb/c mouse 80–90 minutes after injection of [^{43}Sc]Sc-HOPO. Approximately 100 μCi of [^{43}Sc]Sc-HOPO was injected.

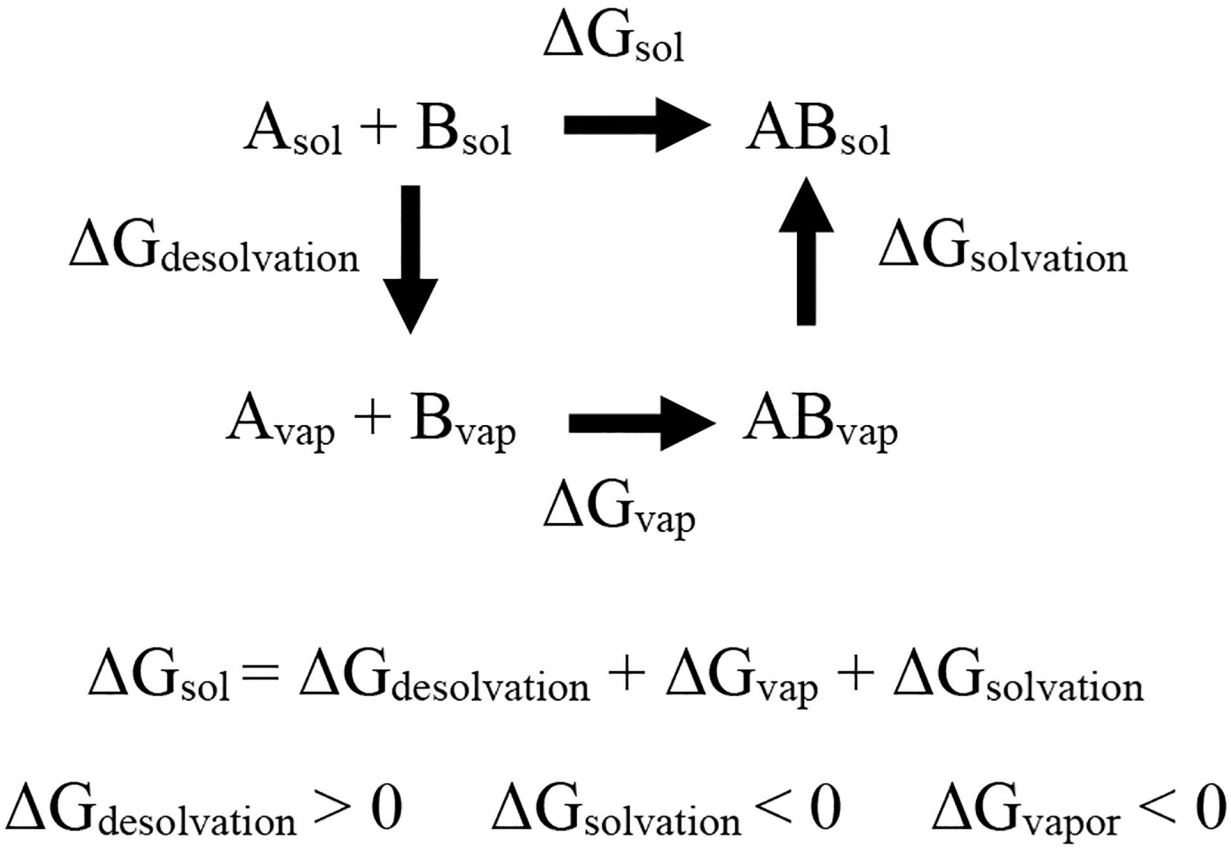

Figure 15.
General thermodynamics cycle used to calculate the change in thermodynamic properties in solution.

Table 1.

Average bond lengths and angles for Sc-HOPO and Sc-HOPOH. $<R_{Sc-O}>$ average Sc and O bond length, R_{OH} is the distance between the H in the protonated hydroxypyridinonate and the O in the adjacent unprotonated hydroxypyridinonate, $A_{O-H\cdots H}$ is the angle between the OH in the protonated hydroxypyridinonate and O in the adjacent unprotonated hydroxypyridinonate

System	$<R_{Sc-O}>$ (Å)	R_{O-H} (Å)	$A_{O-H...H}$ (Degrees)
8-coordinate Complex A	2.25(2)		
7-coordinate Complex B	2.19(2)	3.02	20°
7-coordinate Complex C	2.19(2)	1.96	15°

Table 2.

Changes in electronic energy, Gibbs free energy, enthalpy, and entropy for formation of complexes defined by reactions 1 and 2.

System	ΔE_e (kcal/mol)	ΔG_s (kcal/mol)	ΔH_s (kcal/mol)	ΔS_s (cal/mol)	HOMO-LUMO Gap (eV)
8-coordinate Complex A	−118.1	−88.8	−52.2	120.0	3.8
7-coordinate Complex B	−30.3	−25.5	−26.5	−3.3	3.7
7-coordinate Complex C	−35.1	−31.0	−32.2	−3.2	4.2